Validation and Implementation of algebraic LES modelling of Scalar Dissipation Rate for reaction rate closure in turbulent premixed combustion

T. Ma[a)], Y. Gao[b)], A.M. Kempf [c)], N. Chakraborty[b) *]

[a)] ERM-Hong Kong Limited, Hong Kong;

[b)] School of Mechanical and Systems Engineering, Newcastle University, UK;

[c)] Lehrstuhl Fluiddynamik, IVG, Institut für Verbrennung und Gasdynamik, Universität Duisburg-Essen, Germany

[*] Corresponding author

ABSTRACT

The closure of the filtered reaction rate of the reaction progress variable using an algebraic model for Favre-filtered Scalar Dissipation Rate (SDR) $\widetilde{N}_c$ in turbulent premixed combustion has been assessed in the context of Large Eddy Simulations (LES). This assessment consists of *a-priori* Direct Numerical Simulation (DNS) analysis based on freely propagating statistically planar turbulent premixed flames and *a-posteriori* analysis, involving the LES simulations of a well-documented rectangular dump combustor configuration with sudden expansion (i.e. ORACLES burner) and a premixed flame stabilised on a triangular bluff body flame holder (i.e. Volvo Rig). It has been found that the newly developed SDR model satisfactorily captures $\widetilde{N}_c$ obtained from explicitly filtered DNS data. The predictions of this SDR based LES closure in the ORACLES burner and Volvo Rig configurations exhibit good agreement with experimental results without requiring any major modification to the model parameters. The predictions of the SDR model for the LES of the ORACLES burner and Volvo Rig have been compared to those of two algebraic Flame Surface Density (FSD) models, which yielded satisfactory agreement with experimental data in a previous analysis. The performance of the SDR based closure remains either comparable to or better than the FSD based closures for the two test configurations considered in this analysis.

Keywords: Scalar Dissipation Rate (SDR), Large Eddy Simulation (LES), Direct Numerical Simulation (DNS), Flame Surface Density (FSD)

NOMENCLATURE

Arabic

A	Amplitude of combustion instability
b, b'	Model parameter
c	Reaction progress variable
c_m	Thermo-chemical parameter for the scalar dissipation rate based reaction rate closure expression
C	Coefficient in the presumed reacting mode probability density function
C_P	Specific heat capacity at constant pressure
C_V	Specific heat capacity at constant volume
C_s	Smagorinsky constant
$C_3, C_4, C_3^*, C_4^*, C_3', C_4', C_3'^*, C_4'^*$	Model parameters
D	Progress variable diffusivity
Da	Damköhler number
Da_L	Local Damköhler number in the context of Reynolds Averaged Navier Stokes simulations
Da_Δ	Sub-grid Damköhler number
D_t	Eddy diffusivity
f_b	Bridging function
f_1	Frequency of combustion instability
$f(c)$	Reacting mode probability density function
G	Filter kernel
h	Backward facing step height of ORACLES burner
H	Flame holder height of Volvo Rig
$\breve{k}$	Turbulent kinetic energy
Ka	Karlovitz number
Ka_L	Local Karlovitz number in the context

	of Reynolds Averaged Navier Stokes simulations
Ka_{Δ}	Sub-grid Karlovitz number
K_c^*	Thermo-chemical parameter in the SDR model
l	Integral length scale
Le	Lewis number
$\vec{M}$	Resolved flame normal vector
M_i	i^{th} component of the resolved flame normal vector
N_c	Scalar dissipation rate
p	Pressure
p_0	Reference pressure
p_1	Model parameter
Pr	Prandtl number
$\vec{r}$	Radial vector
Re_t	Turbulent Reynolds number
Re_{Δ}	Sub-grid turbulent Reynolds number
S_d	Displacement speed
S_L	Unstrained laminar burning velocity
Sc	Schmidt number
S_{ij}	Components of strain rate tensor
t	Time
t_{chem}	Chemical time scale
t_f	Initial turbulent eddy turnover time
t_{sim}	Simulation time
T	Temperature
T_{ad}	Adiabatic flame temperature
T_0	Unburned gas temperature
T_b	Burned gas temperature

u_i	i^{th} component of fluid velocity
u'	Root mean square velocity fluctuation magnitude
u'_Δ	Sub-grid turbulent velocity fluctuation
U_{fluct}	Artificial velocity fluctuations at the inlet
U_0	Mean axial velocity
$\dot{w}$	Chemical reaction rate of reaction progress variable
x	Axial co-ordinate
x_i	i^{th} Cartesian co-ordinate
z	Transverse co-ordinate

Greek

α_{T0}	Thermal diffusivity in unburned gas
β	Zel'dovich number
$\beta_1, \beta_c, \beta'_1, \beta'_c$	Model parameters
Γ	Efficiency function
δ_z	Zel'dovich thickness
δ_{th}	Thermal flame thickness
Δ	Filter width
Δ_m	DNS mesh size
$\breve{\varepsilon}$	Dissipation rate of turbulent kinetic energy in the context of Reynolds Averaged Navier Stokes simulations
ε_c	Unresolved component of scalar dissipation rate in the context of Reynolds Averaged Navier Stokes simulations
γ	Ratio of specific heat capacities
λ	Thermal conductivity
μ_0	Dynamic viscosity of unburned gas
ν_t	Eddy kinematic viscosity
ν_u	Kinematic viscosity of unburned gas

ρ	Gas density
ρ_0	Unburned gas density
Σ_{gen}	Generalised Flame Surface Density
τ	Heat release parameter
θ	Model parameter
Θ	Empirical model parameter linking $\bar{c}$ to $\tilde{c}$
Φ	Equivalence ratio
Ξ	Wrinkling factor for Flame Surface Density
Ξ_D	Wrinkling factor for scalar dissipation rate
Ξ_D^V	Wrinkling factor for scalar dissipation rate based on volume averaged quantities

Symbol

$\bar{q}$	Large Eddy Simulation filtered value of a general quantity q
$\tilde{q}$	Favre filtered value of a general quantity q
$\breve{q}$	Favre mean value of a general quantity q
q''	Favre fluctuation of a general quantity q
$< q >$	Reynolds averaged value of a general quantity q
$[q]_L$	Planar laminar flame value of a general quantity q
$\{q\}_V$	Volume averaged value of a general quantity q
$\overline{(q)}_s$	Surface-weighted filtered value of a general quantity q

Acronyms

CARS	Coherent Anti-Stokes Raman Scattering
CDS	Central Differencing Scheme
CFL	Courant-Friedrichs-Lewy
CGT	Counter-gradient transport
DNS	Direct Numerical Simulation
FSD	Flame Surface Density
KPP	Kolmogorov-Petrovsky-Piskunov

LDV	Laser Doppler Velocimetry
LES	Large Eddy Simulation
RANS	Reynolds Averaged Navier Stokes
SDR	Scalar Dissipation Rate
TVD	Total Variation Diminishing
UDS	Upwind Differencing Scheme

1. INTRODUCTION

In turbulent premixed combustion the scalar field is often represented by a reaction progress variable c, which can be defined in terms of a suitable species mass fraction or temperature. In the context of Reynolds Averaged Navier Stokes (RANS) and Large Eddy Simulations (LES) the modelling of premixed turbulent combustion translates to the modelling of the reaction rate and sub-grid scalar flux terms. Thus, the development of high-fidelity reaction rate closures plays a key role in obtaining improved predictions of heat release and pollutant generation rates in premixed turbulent flames, which in turn helps designing new-generation energy-efficient and environment-friendly combustion devices. The recent advances in high performance computing have made LES simulations more affordable and it is anticipated that LES will play an increasingly important role in the future. A number of different methodologies exist for turbulent premixed combustion modelling. The level-set (*G*-equation, Ref. [1]), Artificially Thickened Flame (ATF, Ref. [2,3]) and Flame Surface Density (FSD, Ref. [4]) closures are amongst the most well-established methods, which have been used successfully in the context of LES in the past. All aforementioned formulations have their own advantages and limitations but they also share important similarities. For example, turbulent flame speed in the level-set (*G*-equation) approach is closely related to the wrinkling factor which plays a pivotal role in the ATF and FSD based closures. Interested readers are referred to Refs. [5,6] for an extensive review of the different closure methodologies in turbulent premixed combustion.

In non-premixed combustion, the rate of mixing and reaction is normally quantified by the Scalar Dissipation Rate (SDR) [7]. Moreover, the mean reaction rate of progress variable remains closely related to the Favre mean value of SDR in the context of RANS simulations according to the following expression [6,8]:

$$< \dot{w} >= \frac{2 < \rho N_c >}{(2c_m - 1)} \tag{1i}$$

In this paper, $< \bullet >$ denotes a Reynolds averaging operation, $\dot{w}$ is the reaction rate of the reaction progress variable c, ρ is the gas density, $N_c = D\nabla c \cdot \nabla c$ is the instantaneous SDR with D being the mass diffusivity of c and the parameter c_m is given by [8]:

$$c_m = \frac{\int_0^1 [c\dot{w}]_L \, f(c) dc}{\int_0^1 [\dot{w}]_L \, f(c) dc} \tag{1ii}$$

where $f(c)$ is the reacting mode probability density function (pdf) of the reaction progress variable *c*, the subscript '*L*' refers to planar laminar flame conditions. It has been demonstrated by Bray [8] that the integrals in Eq. (1ii) can be evaluated using the laminar flame data, and that the assumption regarding the smooth function approximating $f(c)$ does not have any significant impact on the numerical value of c_m, which remains between 0.7-0.9 for typical hydrocarbon-air mixtures. Thus c_m can be considered as a thermo-chemical parameter, representing the reaction rate weighted progress variable for unstrained laminar flames.

Recently Chakraborty and Cant [9] demonstrated that Eq. (1i) remains valid for a range of different Lewis numbers Le, provided that the SDR is appropriately modelled. Moreover, the SDR closure inherently provides the rate of micro-mixing, which is also beneficial for the modelling of scalar-variance transport. Furthermore, the SDR based closure naturally links energy and species transport without making strong assumptions unlike the level-set approach. The aforementioned attributes make the SDR based closure a promising methodology for reaction rate modelling in turbulent premixed combustion. A number of previous *a-priori* DNS analyses [10-21] concentrated on the development of SDR closures for turbulent premixed combustion in the context of RANS simulations, and promising results have been obtained based on *a-posteriori* validation using actual RANS simulations [22-24]. This necessitates an extension of the SDR based closures for LES simulations, which has rarely been addressed in detail in the existing literature. A recent *a-priori* DNS analysis by Dunstan *et al.* [25] demonstrated that Eq. (1i) can be recast in the following form for the purpose of LES:

$$\overline{\dot{w}} = \frac{2\overline{\rho}\widetilde{N}_c}{(2c_m - 1)} \tag{2}$$

where for a general quantity q, in this paper, the LES filtered (unweighted) and Favre filtered values are denoted by $\overline{q}$ and $\widetilde{q} = \overline{\rho q}/\overline{\rho}$ respectively. Furthermore, Dunstan *et al.* [25] found that Eq. (2) could be used to predict $\overline{\dot{w}}$ for the purpose of most practical LES where the filter width Δ remains much greater than the thermal flame thickness $\delta_{th} = (T_{ad} - T_0)/\max[|\nabla T|]_L$. Dunstan *et al.* [25] also extended the algebraic SDR model, which was originally proposed by Kolla *et al.* [18] for RANS, to make it suitable for LES of premixed flames with unity Lewis number (i.e. $Le = \lambda/\rho C_p D = 1.0$).

Chakraborty and Swaminathan [20] extended the algebraic RANS-SDR model proposed by Kolla *et al.* [18] for non-unity Le flames. Gao *et al.* [26] extended this RANS model for LES, accounting for the different values of heat release parameter τ, global Lewis number Le and turbulent Reynolds number Re_t. The model was assessed using *a-priori* DNS analysis by Gao *et al.* [26] that demonstrated how the new model captures $\widetilde{N}_c$ behaviour for a range of filter widths Δ. It remains however necessary to assess the model performance in an actual LES because the implications of the numerical implementation and its interaction with the LES turbulence modelling cannot be ascertained solely based on *a-priori* assessment: in actual LES, the modelling and numerical inaccuracies may interact in a complicated manner leading to accurate (erroneous) predictions if these inaccuracies cancel (augment) each other. This necessitates a comprehensive *a-posteriori* assessment of the algebraic SDR closure based on actual LES simulations, which is undertaken in the present work. It is worth noting that this analysis is one of the first attempts in this regard.

A well-documented rectangular dump combustor configuration with sudden expansion (ORACLES burner) [27] and a flame stabilised on a triangular bluff body within a rectangular channel (Volvo Rig) [28-30] have been chosen for the purpose of *a-posteriori* analysis of the algebraic SDR based filtered reaction rate closure in this paper. The latter test case, in particular, offers additional information on temperature, which adds greater value to the analysis, as the levels of heat release and flame location can be identified in a better manner. The LES simulations have been carried out based on the numerical implementation that has been used by Ma *et al.* [28] for *a-posteriori* assessment of

several algebraic FSD models for LES. As $\tilde{N}_c = \overline{\rho D \nabla c \cdot \nabla c} / \bar{\rho}$ is closely related to the generalised FSD $\Sigma_{gen} = \overline{|\nabla c|}$ [25,28,31] due to the dependency on the reactive scalar gradient ∇c, it is useful to compare the performance of the SDR based closure to the best algebraic FSD models identified in the previous analysis [28].

The main objectives of the present analysis are:

(i) To assess and validate an algebraic model of $\tilde{N}_c$ based on *a-priori* analysis of DNS data of statistically planar flames and *a-posteriori* analysis based on the LES of two real test cases - the Volvo rig and the Oracles burner.

(ii) To compare the performance of the algebraic SDR based filtered reaction rate closure for LES with two algebraic FSD models which were found to perform well in a previous analysis [28].

The rest of the paper will start with the necessary mathematical background. Following this, results based on both *a-priori* and *a-posteriori* assessments will be presented and subsequently discussed. The main findings will be summarised and conclusions will be drawn in the final section of this paper.

2. MATHEMATICAL BACKGROUND

In turbulent premixed flames the species field is often characterised by a reaction progress variable c that rises monotonically from 0 in unburned reactants to 1 in fully burned products. The transport equation of the Favre filtered reaction progress variable $\tilde{c}$ takes the following form:

$$\overline{\rho}\left[\frac{\partial \tilde{c}}{\partial t}+\tilde{u}_j\frac{\partial \tilde{c}}{\partial x_j}\right]=\overline{\frac{\partial}{\partial x_j}\left[\rho D\frac{\partial c}{\partial x_j}\right]}+\overline{\dot{w}}-\frac{\partial}{\partial x_j}[\overline{\rho u_j c}-\overline{\rho}\tilde{u}_j\tilde{c}] \quad (3)$$

The two terms on the left hand side (LHS) of Eq. (3) indicate the transient and the resolved advection effects. The terms on the right hand side (RHS) denote the filtered molecular diffusion, chemical reaction rate and the sub-grid turbulent transport of the reaction progress variable respectively. The filtered reaction rate $\overline{\dot{w}}$, the filtered diffusion term $\overline{\nabla\cdot(\rho D\nabla c)}$ and the turbulent transport term $-\partial[\overline{\rho u_j c}-\overline{\rho}\tilde{u}_j\tilde{c}]/\partial x_j$ are unclosed and thus need to be modelled in LES. According to the generalised FSD based closure, the combined contribution of $\overline{\dot{w}}$ and $\overline{\nabla\cdot(\rho D\nabla c)}$ is modelled in the following manner [31]:

$$\overline{\dot{w}}+\overline{\nabla\cdot(\rho D\nabla c)}=\overline{(\rho S_d)}_s\Sigma_{gen} \quad (4)$$

In Eq. (4) $S_d=(Dc/Dt)/|\nabla c|$ is the displacement speed. For the corrugated flamelets (CF) regime, where the flame thickness is smaller than the Kolmogorov length scale, $\overline{(\rho S_d)}_s$ can be modelled as: $\overline{(\rho S_d)}_s=\rho_0 S_L$, which leads to the following form of the modelled transport equation for $\tilde{c}$:

$$\overline{\rho}\left[\frac{\partial \tilde{c}}{\partial t}+\tilde{u}_j\frac{\partial \tilde{c}}{\partial x_j}\right]=\underbrace{\rho_0 S_L\Xi|\nabla\overline{c}|}_{=\rho_0 S_L\Sigma_{gen}}-\frac{\partial}{\partial x_j}[\overline{\rho u_j c}-\overline{\rho}\tilde{u}_j\tilde{c}] \quad (5)$$

In this equation, $\Xi=\Sigma_{gen}/|\nabla\overline{c}|$ denotes the wrinkling factor. Interested readers can refer to previous work [28,32-34] for a detailed account of the many available wrinkling factor models and the assessment of their performances.

Several previous analyses [35-55] demonstrated that the conventional gradient hypothesis model (i.e. $[\overline{\rho u_j c}-\overline{\rho}\tilde{u}_j\tilde{c}]=-\overline{\rho}D_t(\partial\tilde{c}/\partial x_i)$, where D_t is the eddy diffusivity) may not

sufficiently capture the behaviour of sub-grid scalar flux $[\overline{\rho u_j c} - \bar{\rho}\tilde{u}_j\tilde{c}]$ and in fact counter-gradient transport (CGT) has been reported. Lecocq *et al.* [52] demonstrated that the model of sub-grid scalar flux $[\overline{\rho u_j c} - \bar{\rho}\tilde{u}_j\tilde{c}] = -\bar{\rho}D_t\partial\tilde{c}/\partial x_i - \Xi\rho_0 S_L(\bar{c}-\tilde{c})M_i$ (where $\vec{M} = -\nabla\bar{c}/|\nabla\bar{c}|$ is the resolved flame normal vector) according to Weller *et al.* [42] leads to the following form of the transport equation of the Favre-filtered reaction progress variable transport equation:

$$\bar{\rho}\left[\frac{\partial\tilde{c}}{\partial t} + \tilde{u}_j\frac{\partial\tilde{c}}{\partial x_j}\right] = \frac{\partial}{\partial x_j}\left[\bar{\rho}(D_t + D)\frac{\partial\tilde{c}}{\partial x_j}\right] + \rho_0 S_L \Xi|\nabla\tilde{c}| \qquad (6)$$

Note that the resolved molecular diffusion term appears in Eq. (6) but not in Eq. (5) because some FSD based closures, (e.g. Muppala *et al.* [56]) model the filtered reaction rate separately as $\overline{\dot{w}} = \rho_0 S_L \Sigma_{gen}$. Equations (5) and (6) indicate that the modelling of the wrinkling factor Ξ plays a key role in the closure of the filtered reaction rate. Ma et al. [28] demonstrated based on a recent analysis on flow configurations, which were used before for model development and assessment [27–30,57,58], that the wrinkling factor (i.e. $\Xi = \Sigma_{gen}/|\nabla\bar{c}|$) models proposed by Fureby [59] and Muppala et al.[56] perform better than the most algebraic FSD models availablein the literature. These models are selected as baseline examples for the comparison against the algebraic SDR based reaction rate closure. For the convenience of discussion, these two FSD models (i.e. Fureby [59] and Muppala *et al.* [56]) will be referred to by the name of the first author throughout this paper. The wrinkling factor expressions, which are going to be considered in this analysis, are given as follows:

<u>FurebyM model</u>:

$$\Xi = \left(1 + \Gamma \frac{u'_\Delta}{S_L}\right)^{D_f - 2} \tag{7i}$$

with $\Gamma = 0.75 \exp\left[-1.2\left(\frac{u'_\Delta}{S_L}\right)^{-0.3}\right]\left(\frac{\Delta}{\delta_z}\right)^{2/3}$ and $D_f = \frac{2.05}{u'_\Delta / S_L + 1} + \frac{2.35}{S_L / u'_\Delta + 1}$ (7ii)

The name 'FurebyM' denotes [28] modified version of Fureby's [59] model to which unity has been added as shown in Eq. (7i). The symbols δ_z and u'_Δ denote the Zel'dovich flame thickness and sub-grid scale velocity fluctuation respectively. The Zel'dovich flame thickness is defined as α_{T0} / S_L, where α_{T0} is the thermal diffusivity in the unburned gas.

Muppala model

$$\Xi = 1 + \frac{0.46}{Le} \mathrm{Re}_\Delta^{0.25} \left(\frac{u'_\Delta}{S_L}\right)^{0.3} \left(\frac{\bar{p}}{p_0}\right)^{0.2} \tag{8}$$

In Eq. (8), $\mathrm{Re}_\Delta = u'_\Delta \Delta / \nu$ is the sub-grid Reynolds number, ν and $\bar{p}$ and p_0 are the kinematic viscosity, filtered pressure and reference pressure respectively.

The model given by Eq. (7i) was used in conjunction with Eq. (5), whereas Eqs. (6) and (8) were used together in the *a-posteriori* assessment by Ma *et al.* [28]. The progress variable diffusivity in Eq. (6) varies with temperature following Sutherland's law [60], while the Schmidt number is kept at a constant value of 0.7. Based on a detailed analysis [28] the sub-grid scalar flux in Eq. (5) can be modelled using the following expression according to Richard *et al.* [61]:

$$[\overline{\rho u_i c} - \bar{\rho} \tilde{u}_i \tilde{c}] = -\bar{\rho} D_t \frac{\partial \tilde{c}}{\partial x_i} - \rho_0 S_L (\bar{c} - \tilde{c}) M_i \tag{9}$$

The turbulent diffusivity D_t in Eq. (9) is expressed as $D_t = \nu_t / Sc_t$ where $Sc_t = 0.7$ is the sub-grid Schmidt number. The eddy kinematic viscosity ν_t can be estimated using the Smagorinsky model [62] and consequently, the parameter u'_Δ in Eqs. (7) and (8) can be evaluated using the following expressions [63,64]:

$$\nu_t = (C_s\Delta)^2(2\tilde{S}_{ij}\tilde{S}_{ij})^{1/2} \quad \text{and} \quad u'_\Delta = \frac{\nu_t}{(C_v\Delta)} \tag{10}$$

In Eq. (10), $\tilde{S}_{ij} = 0.5(\partial\tilde{u}_i/\partial x_j + \partial\tilde{u}_j/\partial x_i)$ is the resolved strain rate tensor, $C_v = 0.1$ is a model parameter and C_s is the Smagorinsky constant [62] (here C_s is taken to be 0.1). The sensitivity of the wrinkling factor based models on C_s has been discussed in Ref. [28] and thus will not be repeated in this paper.

The filtered (unweighted) progress variable $\bar{c}$ needs to be evaluated from the readily available $\tilde{c}$. Chakraborty and Cant [65] proposed an expression based on the BML formulation [66]: $\bar{c} = [(1+\tau)\tilde{c}]/[1+\tau\tilde{c}]$ to account for $\bar{c} \to \tilde{c}$ in the limit of $\Delta \to 0$. The expression suggested by Chakraborty and Cant [65] reads:

$$\bar{c} = \frac{(1+\tau)\tilde{c}}{1+\tau\tilde{c}}\left(1-\exp\left(-\Theta\frac{\Delta}{\delta_L}\right)\right)+\tilde{c}\exp\left(-\Theta\frac{\Delta}{\delta_L}\right) \tag{11}$$

In Eq. (11) $\Theta = 0.2$ is an empirical model parameter and $\delta_L = 1/Max\left|\nabla c\right|_L$ is an alternative flame thickness based on the reaction progress variable gradient [65].

According to the SDR based closure, the filtered reaction rate $\overline{\dot{w}}$ is modelled using Eq. (2):

$$\bar{\rho}\left[\frac{\partial \tilde{c}}{\partial t}+\tilde{u}_j\frac{\partial \tilde{c}}{\partial x_j}\right]=\frac{\partial}{\partial x_j}\left[\bar{\rho}\tilde{D}\frac{\partial \tilde{c}}{\partial x_j}\right]+\frac{2\bar{\rho}\tilde{N}_c}{(2c_m-1)}-\frac{\partial}{\partial x_j}[\overline{\rho u_j c}-\bar{\rho}\tilde{u}_j\tilde{c}] \qquad (12)$$

Dunstan *et al.* [25] extended the RANS model for SDR by Kolla *et al.* [18] in the following manner to model $\tilde{N}_c$:

$$\tilde{N}_c=\tilde{D}\nabla\tilde{c}\cdot\nabla\tilde{c}+\left[1-\exp\left(-\theta\frac{\Delta}{\delta_{th}}\right)\right]\left[2K_c^*\frac{S_L}{\delta_{th}}+(C_3-\tau C_4 Da_\Delta)\frac{2u'_\Delta}{3\Delta}\right]\frac{\tilde{c}(1-\tilde{c})}{\beta_1} \qquad (13i)$$

with $\theta=0.75$; $C_3=\dfrac{1.5\sqrt{Ka_\Delta}}{1+\sqrt{Ka_\Delta}}$; $C_4=\dfrac{1.1}{(1+Ka_\Delta)^{0.4}}$ and $\beta_1=2.4$ (13ii)

In Eqs. (13i) and (13ii), $Da_\Delta=\Delta S_L/u'_\Delta\delta_{th}$ and $Ka_\Delta=(u'_\Delta/S_L)^{3/2}(\Delta/\delta_{th})^{-1/2}$ are the local sub-grid Damköhler and Karlovitz numbers respectively, where $\delta_{th}=(T_{ad}-T_0)/Max|\nabla T|_L$ with subscript L referring to the unstrained planar laminar flame quantities. The parameter K_c^* in Eq. (13i) is given by [15,18,67]:

$$K_c^*=\frac{\delta_{th}}{S_L}\frac{\int_0^1[\rho N_c\nabla\cdot\vec{u}]_L f(c)dc}{\int_0^1[\rho N_c]_L f(c)dc} \qquad (14i)$$

In Eq. (14i) $[\rho N_c\nabla\cdot\vec{u}]_L$ and $[\rho N_c]_L$ can be obtained from unstrained laminar flame calculations and the reacting mode pdf $f(c)$ can be approximated as $f(c)=C/|\nabla c|_L$ [6] where C is a coefficient obtained using the following normalisation [6,18,67]:

$$\int_0^1 f(c)dc=C\int_{0.001}^{0.999}\frac{dc}{|\nabla c|_L}=1.0 \qquad (14ii)$$

Equations (13iii) and (13iv) suggest that K_c^* is a thermo-chemical parameter which provides the value of SDR-weighted dilatation rate $\nabla\cdot\vec{u}$.

The function $[1-\exp(-\theta\Delta/\delta_{th})]$ in Eq. (13i) ensures that $\widetilde{N}_c$ approaches $D\nabla c\cdot\nabla c$ when the flow is fully resolved (i.e. $\Delta\to 0$). The function $[1-\exp(-\theta\Delta/\delta_{th})]$ and the first term on the right hand side of Eq. (13i) were absent in the original model by Kolla *et al*. [18] as the RANS model was proposed only for the unresolved part of SDR:

$$\breve{\varepsilon}_c = \breve{N}_c - \breve{D}\nabla\breve{c}.\nabla\breve{c} \qquad (15)$$

where $\breve{q} = <\rho q>/<\rho>$ and $q'' = q-\breve{q}$ are the Favre-mean and Favre-fluctuation of a general quantity q respectively. The physical basis of the RANS model of $\breve{\varepsilon}_c$ by Kolla *et al.* [18] is summarised in Appendix A. The model given by Eq. (13i) and the original model proposed by Kolla *et al.* [18] are strictly valid only for unity Lewis number flames. Moreover, Eq. (13i) was proposed based on the *a-priori* analysis of a single V-flame DNS database with $Le=1.0$. Recently, Gao *et al.* [26] have extended Eq. (13i) for the purpose of modeling $\widetilde{N}_c$ in the context of LES so that it can account for non-unity Lewis number effects, following the modification to the $\breve{\varepsilon}_c$ model suggested by Chakraborty and Swaminathan [20] (see Eq. (A7) in Appendix A). The LES SDR model by Gao *et al.* [26] takes the following form:

$$\widetilde{N}_c = \widetilde{D}\nabla\widetilde{c}.\nabla\widetilde{c} + (1-f_b)\left[\frac{2K_c^*S_L}{Le^{1.88}\delta_{th}} + (C_3^* - \tau Da_\Delta C_4^*)\frac{2u'_\Delta}{3\Delta}\right]\frac{\widetilde{c}(1-\widetilde{c})}{\beta_c} \qquad (16)$$

with $f_b = \exp[-\theta(\Delta/\delta_{th})^{p_1}]$ is a bridging function, C_3^*, C_4^* and β_c are the model parameters [20]:

$$C_3^* = \frac{2.0\sqrt{Ka_\Delta}}{(1.0+\sqrt{Ka_\Delta})};\ C_4^* = \frac{1.2(1.0-\widetilde{c})^b}{[Le^{2.57}(1+Ka_\Delta)^{0.4}]}\ \text{ where } b = 0.2+1.5|1.0-Le| \qquad (17)$$

The first term on the RHS of Eq. (16) and the bridging function $(1-f_b)$ in the second term were absent in the RANS model [20] (see Eq. (A7)). The second term on the RHS of Eq. (16) (without $(1-f_b)$) can be derived in the context of RANS based on the equilibrium of leading order source and sink terms of the transport equation of $\breve{\varepsilon}_c$ (see discussion in Appendix A). The bridging function $(1-f_b)$ ensures that $\widetilde{N}_c$ approaches $N_c = D\nabla c \cdot \nabla c$ for small values of filter size (i.e. $\lim_{\Delta\to 0} \widetilde{N}_c = N_c = D\nabla c \cdot \nabla c$ where $f_b \approx 1.0$), whereas Eq. (16) reverts back to the RANS model expression (i.e. Eq. (A7)) for $\Delta >> \delta_{th}$. The expressions of $C_3'^*$, $C_4'^*$ and b' in Eq. (A8) have been extended from RANS to LES to obtain C_3^*, C_4^* and b in Eq. (17). The involvement of the bridging function $(1-f_b)$ in Eq. (16) and using the SDR closure in LES context, may alter the value of β_c in comparison to β_1'. It is worth noting that the model parameters C_3^* and C_4^* are three-dimensional variables in the context of LES, so for the sake of simplicity in terms of modelling and optimisation of model parameters, β_c is considered to be constant for a given thermo-chemistry. Moreover, this makes it convenient to analyse the influence of β_c on SDR $\widetilde{N}_c$ prediction independent of turbulence modelling (unlike C_3^* and C_4^*, because the modelling of u_Δ' is likely to affect these parameters). A similar approach was adopted previously by Dunstan *et al.* [25]. The evaluation of β_c, its parameterisation, and the sensitivity of β_c on the prediction of LES simulations will be discussed in Sections. 3.2 and 4.2 later in this paper.

The predictions of Eq. (13i) and Eq. (16) remain comparable for unity Lewis number flames. The model given by Eq. (16) can be substituted into Eq. (12) to provide closure to the LES filtered reaction rate, and the sub-grid scalar flux is modelled using Eq. (9). Note that the thermal flame thickness in Eq. (16) is evaluated using the relation $\delta_{th}/\delta_z = 2(1+\tau)^{0.7}$ [14,18,68] for LES simulations.

The modelling methodologies considered in this analysis are summarised in Table 1 for the sake of quick reference for the readers and future potential users of these models.

3. *A-PRIORI* DNS ANALYSIS

3.1 DNS database and numerical implementation

The *a-priori* DNS assessment of the model given by Eq.(16) is conducted using a DNS database of statistically planar turbulent premixed flames with global Lewis number ranging from $Le = 0.34$ to 1.2. This database has been used to gain fundamental understanding in modelling the effects of τ and *Le* on turbulent kinetic energy [69,70], scalar flux [49-51], FSD [9,33], scalar variance [20], and SDR [20] in the context of RANS and LES simulations. A brief summary of the attributes of this database is provided here and further details of this database are available in Refs. [9,20,33,49,51,69,70]. The initial values of the root-mean-square (rms) turbulent velocity fluctuation normalised by unstrained planar laminar burning velocity u'/S_L and the integral length scale to flame thickness ratio l/δ_{th} for cases A-F are presented in Table 2 along with the values of Damköhler number $Da = lS_L/u'\delta_{th}$, Karlovitz number $Ka = (u'/S_L)^{3/2}(l/\delta_{th})^{-1/2}$, turbulent Reynolds number $\mathrm{Re}_t = \rho_0 u' l/\mu_0$, heat release

parameter $\tau = (T_{ad} - T_0)/T_0$ and Lewis number *Le*. Standard values are taken for Prandtl number Pr, ratio of specific heats $\gamma = C_p/C_v$ and the Zel'dovich number $\beta = T_{ac}(T_{ad} - T_0)/T_{ad}^2$ (i.e. $\mathrm{Pr} = 0.7, \gamma = 1.4, \beta = 6.0$). The values of c_m for cases A-F are found to be 0.85, 0.92, 0.87, 0.867, 0.825 and 0.816 respectively, whereas $K_c^*/\tau = 0.756$, 0.52, 0.67, 0.71, 0.78, 0.79 respectively for cases A-F. The aforementioned values of c_m and K_c^*/τ have been evaluated using $f(c) = C/|\nabla c|_L$ and unstrained planar laminar flame solutions.

The domain of size $24.1\delta_{th} \times 24.1\delta_{th} \times 24.1\delta_{th}$ is considered for cases A-F. A Cartesian mesh of size $230 \times 230 \times 230$ with uniform mesh spacing in each direction is used for all cases. The spatial derivatives are evaluated using a 10th order central-difference scheme for the internal grid points and the order of differentiation drops gradually to one-sided second order scheme near non-periodic boundaries. A 3rd order low storage Runge-Kutta method is used for explicit time advancement. The simulations for cases A-F are carried out for about three initial eddy turn over times (i.e. $t_{sim} = 3.34t_f = 3.34l/u'$) which is equal to one chemical time scale $t_{chem} = \delta_{th}/S_L$ for these cases. This simulation time remains either comparable to or greater than several previous analyses [31,40,41,45,48,71-76]. The values of u'/S_L in the unburned reactants ahead of the flame at the time when statistics were extracted decreased by about 50%, of the initial values, whereas the values of l/δ_{th} have increased from their initial values by a factor of about 1.7, but there are still enough turbulent eddies on the burned and unburned side of the flame. The flamelet assumption remains valid for both the initial and final values of

u'/S_L and l/δ_{th} in all cases considered here according to the regime diagram by Borghi and Peters [1].

The DNS data is explicitly filtered using a Gaussian filter kernel: $G(\vec{r}) = (6/\pi\Delta^2)^{3/2} \exp(-6\vec{r}\cdot\vec{r}/\Delta^2)$ [25,31,33,44,47,71] to obtain the relevant filtered quantities for the present analysis. In the next section the results will be presented for Δ ranging from $\Delta = 4\Delta_m \approx 0.4\delta_{th}$ to $\Delta = 28\Delta_m \approx 2.8\delta_{th}$, where Δ_m is the DNS mesh size $(\Delta_m \approx 0.1\delta_{th})$. These filter sizes are comparable to the range of Δ explored in *a-priori* DNS analysis in several previous studies [25,31,33,44,47,71], and span a useful range of length scales (i.e. from Δ comparable to $0.4\delta_{th}$ where the flame is partially resolved, up to $2.8\delta_{th}$ where the flame becomes fully unresolved and Δ is comparable to the integral length scale) (see Table 2).

3.2. Results and Discussion

The variations of the mean values of the normalised chemical source term $\overline{\dot{w}} \times \delta_{th}/\rho_0 S_L$ and the modelled normalised source term $2\overline{\rho}\widetilde{N}_c/(2c_m - 1) \times \delta_{th}/\rho_0 S_L$ conditional on $\widetilde{c}$ values for $\Delta \approx 0.8\delta_{th}$, $\Delta \approx 1.6\delta_{th}$ and $\Delta \approx 2.8\delta_{th}$ for cases A-F are shown in Fig. 1. This is done in order to assess the applicability of Eq. (2) in the context of LES for different values of τ and Le. It is evident from Fig. 1 that the modelled source term does not satisfactorily predict the real source term for very fine grids (i.e. $\Delta < \delta_{th}$), but that the

agreement improves with increasing filter width (i.e. $\Delta > \delta_{th}$), which matters for real LES.

The expression $< \dot{w} >= 2 < \rho N_c > /(2c_m - 1)$ was originally proposed for $Da >> 1$ where the pdf of c shows higher probability of finding either unburned or fully burned gases than finding burning mixtures [8]. In order to explain the discrepancy between the chemical source term and its model for small values of Δ, it is useful to analyse the behaviour of Da_Δ and the sub-grid pdf of c. The variations of Da_Δ conditional on $\tilde{c}$ values for different values of Δ are shown in Fig. 2 for cases A-F. The pdfs of c within the filter volume at $\tilde{c} = 0.5$ at different filter widths for cases A-F are shown in Fig. 3. A comparison between Figs. 1-3 demonstrates that the agreement between the chemical source term and its model improves with increasing Da_Δ when there is a significant probability of finding $c \neq \tilde{c}$ within the filter volume. This observation is found to be consistent with previous findings [25,26]. However, Fig. 1 demonstrates that Eq. (2) can be used for the closure of $\overline{\dot{w}}$ for most practical LES simulations where Δ often assumes much greater values than $2.8\delta_{th}$ (i.e. $\Delta >> 2.8\delta_{th}$). However, the accuracy of the model for the chemical source term (i.e. Eq. (2)) for $\Delta >> \delta_{th}$ depends on accurate modelling of $\tilde{N}_c$.

In actual LES simulations u'_Δ needs to be modelled and thus the modelling inaccuracies associated with u'_Δ are also likely to affect the evaluation of Da_Δ, Ka_Δ and the model

parameters C_3^* and C_4^*, which in turn can affect the accuracy of the SDR model (i.e. Eq. (16)). In order to ensure both *a-priori* and *a-posteriori* analyses are consistent with each other, the performance of the SDR model (i.e. Eq. (16)) is assessed for both u'_Δ extracted from DNS data, and for u'_Δ prediction according to the model given by Eq. (10).

The relative contributions of sub-grid and resolved components of SDR can be quantified with the help of a wrinkling factor based on SDR, which can be defined as [25]:

$$\Xi_D = \frac{\overline{\rho}\widetilde{N}_c}{\overline{\rho}\widetilde{D}\nabla\widetilde{c}\cdot\nabla\widetilde{c}} \tag{18}$$

As $\overline{\dot{w}}$ can be considered to be directly proportional to $\overline{\rho}\widetilde{N}_c$ for a given thermo-chemistry according to Eq. (2), the volume-averaged value of density-weighted SDR $\left\{\overline{\rho}\widetilde{N}_c\right\}_V$ should remain independent of Δ, where $\left\{Q\right\}_V$ is the volume-averaged value of a general quantity Q. The variation of the wrinkling factor Ξ_D^V based on the volume-averaged quantities ($\Xi_D^V = \left\{\overline{\rho}\widetilde{N}_c\right\}_V \Big/ \left\{\overline{\rho}\widetilde{D}\nabla\widetilde{c}\cdot\nabla\widetilde{c}\right\}_V$) with changing Δ/δ_{th} is shown in Fig. 4 for cases A-F. It is found that Eq. (16) captures the variation of Ξ_D^V with Δ/δ_{th} for $f_b = \exp[-0.7(\Delta/\delta_{th})^{1.7}]$ provided that an optimum value of β_c (i.e. 3.3 for case A and 4.35 for cases B-F) is used, and u'_Δ is extracted from DNS data. However, it is found that Eq. (16) also captures the variation of Ξ_D^V with Δ/δ_{th} for $f_b = \exp[-0.7(\Delta/\delta_{th})^{1.7}]$ when u'_Δ is evaluated using Eq. (10) and β_c assumes the value 2.86 and 3.7 for cases A and B-F respectively.

The main purpose of Fig. 4 is to obtain the optimum value of β_c for which Eq. (16) captures the variation of Ξ_D^V with changing Δ and not to compare the performances of FurebyM and Muppala models with the SDR based closure discussed here. The wrinkling factor $\Xi_V = \{\Sigma_{gen}\}_V / \{|\nabla \bar{c}|\}_V$ based on volume-integrated values of generalised FSD Σ_{gen} and its resolved component is fundamentally different from $\Xi_D^V = \{\bar{\rho}\tilde{N}_c\}_V / \{\bar{\rho}\tilde{D}\nabla\tilde{c}\cdot\nabla\tilde{c}\}_V$ in spite of close relation between $\tilde{N}_c$ and Σ_{gen}. The quantity Ξ_D^V represents the degree of unresolvedness of SDR, whereas Ξ_V provides the measure of flame surface wrinkling as $\{\Sigma_{gen}\}_V$ represents the flame surface area. Moreover, the statistical behaviours of Ξ_V for the DNS cases considered here have been presented elsewhere (see Fig. 1b of Ref. [32] for case A and Fig. 1 of Ref. [34] for cases B-G) and thus are not repeated here in Fig. 4. Furthermore, the performance of the wrinkling factor Ξ for FSD based closure was assessed in earlier publications by the current authors (see Figs. 2-4 and Table IV in Ref. [32] for case A; Figs. 3-8 for cases B-G and Figs. 23a and 23b of Ref. [28] for ORACLES rig and VOLVO rig respectively) and thus are not repeated here. As the main focus of the current analysis is to compare the performance of the newly developed SDR closure with the two best FSD based closures identified in an earlier analysis [28], interested readers are referred to Refs. [28,32,34] for further information on Ξ and the performances of its models including the FurebyM and Muppala models.

The variation of mean values of $\tilde{N}_c$ conditional on $\tilde{c}$ obtained from DNS data is compared to the prediction of Eq. (16) for $f_b = \exp[-0.7(\Delta/\delta_{th})^{1.7}]$ in Fig. 5 where $\beta_c = 3.3$ (4.35) is used for case A (cases B-F) when u'_Δ is extracted from DNS data,

whereas $\beta_c = 2.86 (3.7)$ is used for case A (cases B-F) when u'_Δ is evaluated using Eq. (10). Figure 5 shows that Eq. (16) satisfactorily captures the qualitative and quantitative variations of $\tilde{N}_c$ across the flame brush for all cases considered here when the optimum value of β_c is used. The optimum values of β_c extracted from DNS data increase with increasing heat release parameter τ. It has been found that Eq. (16) captures the variation of Ξ_D^V with Δ / δ_{th} for the $\tau = 2.52$ V-flame considered by Dunstan *et al.* [25] when u'_Δ is extracted from DNS data (not shown here). Chakraborty *et al.* [15] demonstrated that β_c must be greater than $2/(2c_m - 1)$ (i.e. $\beta_c \geq 2/(2c_m - 1)$) in order to satisfy the physical realisability (i.e. $\widetilde{N}_c \geq 0$). This realisability criterion and the optimum value of β_c extracted from DNS, when u'_Δ is evaluated using Eq. (10), has been parameterised here in the following manner for C_s=0.1:

$$\beta_c = \max\left(\frac{2}{2c_m - 1}, \left[1.1\frac{\tau}{\tau + 1} + 0.41 \right]^{4.9} \right) \tag{19}$$

It is worth noting Eq. (19) parameterises not only optimum values of β_c for cases A-F (i.e. for $\tau = 3.0$ and 4.5) but also remains valid for the $\tau = 2.52$ flame considered by Dunstan *et al*. [25]. According to Eq. (19) β_c assumes an asymptotic value (i.e. $\beta_c = 7.5$ for $t \to \infty$) and this asymptotic value remains close to the value of $\beta'_c = 6.7$ proposed by Chakraborty and Swaminathan [20] in the context of RANS. The predictions of Eq. (16) for β_c given by Eq. (19) are shown in Figs. 4 and 5, which demonstrate that both the wrinkling factor Ξ_D^V and the SDR $\widetilde{N}_c$ are predicted accurately for the β_c parameterisation given by Eq. (19).

4. *A-POSTERIORI* ANALYSIS

4.1. Experimental configurations

The plane symmetric dump combustor known as the ORACLES burner is a well-documented test case for which measurements were conducted by Nguyen *et al.* [27] and Besson *et al.* [77], and simulations were carried out by several computational groups [78-80] employing different methods of premixed combustion modelling. Interested readers can refer to Nguyen *et al.* [27] for a comprehensive description of the whole (of size ≈6m) burner. Figure 6 shows a 2-D sketch on the area of interest or computational domain, which in the horizontal direction, stretches from the tip of the splitter plate with an opening angle of 14° down to a normalised distance of $x/h = 14$, where h represents the step height of 29.9 mm and the origin of x lies at the location of the sudden geometric expansion known as the dump combustor plane. Upstream of the computational domain are two 3m long rectangular channels that transport lean mixtures of propane-air at the same equivalence ratio of $\Phi = 0.75$ for the current test configuration, while the burned gases escape via an exhaust section in the downstream section of the domain. The experimental data consists of instantaneous direct light visualisations of the flame and mean and fluctuating velocities, which were measured using Laser Doppler Velocimetry (LDV) [27] at six different vertical lines. The experimental parameters that are relevant for the *a-posteriori* analysis are presented in Table 3, where the Reynolds number Re is defined based on the bulk velocity U_0, h and the unburned gas kinematic viscosity v_u. It is worth noting that a streamwise pulsation of 50Hz was observed in the experiments by Nguyen *et al.* [27] as induced by the complex interaction of vortices shed behind the

backward facing steps and splitter plate with the premixed flame. The emulation of this behaviour in the numerical simulation is discussed in Section 4.2.

The Volvo Rig is another test case that has been extensively used in the development and testing of combustion models [28-30,64,81-83]. However, unlike the ORACLES burner, the test case provides additional information on temperature, which is important in defining the flame location and levels of heat release. The velocity and temperature data were measured by Sjunnesson *et al.* [29, 84] using Laser Doppler Anemometry (LDA) and Coherent Anti-Stokes Raman Scattering (CARS) respectively. Figure 7 shows a sketch of the combustor section of the Volvo Rig, primarily consisting of a triangular bluff body or flame holder with its right most vertical side located at an axial distance of 0.31m from the inlet of a 1m long rectangular channel. The recirculation of the burned gas behind the flame holder helps to stabilise the flame, while the turbulence generated within the shear layers behind the bluff body enhances the mixing of gases and increases the rate of burning. For this geometric set up, two different operating conditions using a lean propane-air mixture were experimentally examined and were found to influence the symmetry of the flame [82]. The operating condition with pre-heated propane air at a temperature of 600K is selected in order to make this analysis consistent with the previous work [28], and the relevant details of these experimental parameters are provided in Table 4. The characteristic length scale for the Reynolds number is chosen to be the flame holder height H of 40mm. The experimental temperature data can be found in the paper by Sjunnesson *et al*. [84], whereas the velocity data can be obtained from the work by Fureby and Möller [30].

4.2 Numerical Implementation

The simulations are performed using an in-house low Mach number solver, 'PsiPhi' [28,85-88] which employs the finite volume (FV) method on a Cartesian grid of cubic cells. Transported variables are stored at cell centres, while velocities are linearly interpolated on cell faces. A Total Variation Diminishing (TVD) scheme with a CHARM limiter is employed for the convective flux of the progress variable and a second-order accurate central differencing scheme (CDS) is used for the advection term of the momentum equation. The implications of applying two different discretisation schemes for the transported scalar and velocity have been discussed by Ma *et al*. [28]. In summary, a CDS scheme is used for momentum transport to ensure low numerical dissipation and finer resolved velocity scales. A TVD scheme is applied for the reactive scalar because a CDS scheme would lead to excessive numerical oscillations that adversely affect flame propagation. However, this use of two different discretisation schemes led to a relatively thicker flame brush as smaller resolved velocity scales are convected in the scalar field, hence thickening the flame brush. The result of applying a TVD scheme for the momentum transport has been presented in the earlier work [28], yielding a relatively thin flame brush but showing that this scheme can be considered too dissipative. A solution to this problem is beyond the scope of the present study. The time integration is carried out using a low storage, third-order accurate Runge-Kutta scheme, in which the total time step width is controlled by the Courant-Friedrichs-Lewy (CFL) criterion based on the convective flow speed, with constant CFL values of 0.3 and 0.5 for the ORACLES burner and Volvo Rig respectively. The solution algorithm is based on a predictor-corrector method [89] with a pressure correction scheme.

In terms of boundary conditions, a no slip-condition is applied at the walls. Chemical reaction is suppressed (set to zero) for fluid cells immediately adjacent to the wall and for all wall cells, which may be considered a simplistic representation of flame quenching due to heat losses. An exception arises for the fluid cells next to the vertical edge of the triangular flame holder of the Volvo Rig, where chemical reactions are enabled in these cells for promoting flame stabilisation. Alternative flame-wall interaction models, for example those used in conjunction with FSD modelling by Keppeler *et al.* [90], are not implemented here because this analysis does not focus on flame-wall behaviour, but rather on a model performance comparison for velocity and temperature quantities at the bulk central regions of the flow. At the outflow, a zero gradient condition is applied for the scalars, while positive outflow is enforced for the axial velocity. For added stability, a blended central/upwind differencing scheme (CDS-UDS) is implemented for velocities 50mm (x/h =12.33) and 80mm (x/H = 15.25) from the outlet boundary for the ORACLES burner and Volvo Rig respectively. These locations lie far away from the last measurement points at x/h = 9 and x/H = 9.40 for the ORACLES burner and Volvo Rig respectively, minimising any adverse numerical influence originating from the outflow.

The stream-wise velocity prescribed at the inlet of the ORACLES burner is given by:

$$u(y,z,t) = U(z)\cdot\left(1 + A\sin(2\pi f_1 t)\right) + U_{fluct}(y,z,t) \tag{20}$$

where $U(z)$ is a mean velocity profile that is fitted by a sixth order polynomial to experimental data at x/h = -5 of the mid y-z plane, and $U_{fluct}(y,z,t)$ represent artificial turbulence fluctuations generated by a method proposed by Klein *et al.* [91] and

subsequently extended by Kempf *et al.* [92]. Equation (20) also shows a sinusoidal velocity component $A\sin(2\pi f_1 t)$ that is used to emulate the combustion instability with amplitude $A = 0.27$ and known frequency $f_1 = 50Hz$ [27]. The selected value of *A* has been adjusted to match the magnitude of the stream-wise velocity fluctuations u' at the dump combustor plane (x/h=0), while the magnitude of U_{fluct} (= 0.836m/s) is approximated to coincide with the experimental transverse velocity fluctuations w'. Coincidentally, the chosen value of *A* is found to lie within the range of values proposed by Duwig and Fureby [80], who have applied similar sinusoidal pulsations in their simulation. For the Volvo Rig, a uniform velocity profile is prescribed at the inlet with a turbulent intensity of 4% of U_0 [84] and integral length scale of 18mm.

Based on a previous grid sensitivity analysis [28], a grid resolution of 2mm is considered for this analysis which leads to 1.60 and 4.5 million cells for the ORACLES burner and Volvo Rig respectively. Normalising the grid resolutions with the corresponding Zel'dovich thicknesses, results in Δ/δ_z values of 14.06 and 12.41 for the ORACLES burner and Volvo Rig respectively. Using the relation $\delta_{th}/\delta_z = 2(1+\tau)^{0.7}$ [14,18,68], Δ/δ_{th} values turn out to be 1.77 and 2.80 for the ORACLES burner and Volvo Rig respectively. It is worth noting that a relatively fine Cartesian grid with cell-aspect ratios of one is used here and thus the evaluation of fluxes is more accurate than applying a similar order discretization scheme on unstructured grids. A central differencing scheme for momentum transport also acts to minimise the effects of numerical diffusion. Furthermore, the FSD models employed here depend on resolved scalar gradient statistics, leading to a flame propagation speed that is rather insensitive against numerical

diffusion as explained in our previous study [28]. The numerical methodology used here was successfully used elsewhere [56, 59, 63, 64, 85, 87, 88]. Moreover, the current grid resolutions also enable consistency with the earlier *a-posteriori* work based on algebraic FSD models [28], in which it was found that finer grids generally resulted in a negligible contribution of the sub-grid model, leading to a less meaningful model comparison. However, this was shown for FSD models but may not be necessarily true for SDR models. A grid sensitivity study using grid resolutions of 2mm and 1mm was therefore carried out and is presented in Appendix B.

The values of K_c^* and c_m are taken to be 0.75τ and 0.85 respectively for LES simulations based on unstrained laminar flame calculations described earlier. The optimum values of β_c in Eq. (16) were found to be approximately 4.6 and 3.3 for the ORACLES burner and Volvo Rig respectively. These values were chosen based on the parameterisation given by Eq. (19), which was proposed based on *a- priori* analysis of DNS data in Section 3.2, where Eq. (16) yielded a satisfactory agreement with DNS data when u'_Δ is evaluated using Eq. (10). This agreement was found to be independent of the values of Le and so should be applicable for the two test configurations, where a lean propane-air mixture has been considered for which the global Lewis number can be taken as $Le = 1.62$ [56]. According to the *a-priori* DNS analysis β_c for the ORACLES burner ($\tau \approx 6.17$) is expected to be greater than in the Volvo Rig ($\tau \approx 2.13$). Another possible reason for the difference in the optimum values of β_c between these two test configurations may arise from the modelling of u'_Δ, where the use of the Smagorinsky model may not be equally accurate for both configurations. There is no consensus on the

optimum value of C_s in the Smagorinsky model, and it is known to vary for different test cases. For example, Germano *et al.* [93] estimated a range of 0.1 to 0.23 for C_s, whereby the lower value was used in turbulent channel flow and the upper value for modelling isotropic turbulence. Manickam *et al.* [83] have applied $C_s = 0.1$ in their reactive simulations of the Volvo Rig. Furthermore, the Smagorinsky model is known to be sensitive to the level of heat release [3]. As a result, the level of modelling uncertainties of u'_{Δ} will differ for each test case. However, further analysis is warranted to ascertain the sensitivity of β_c on u'_{Δ} modelling. For the sake of completeness, a sensitivity study of the β_c for the two test configurations is discussed in Appendix C.

4.3 Results and Discussion

4.3.1. ORACLES burner

Figure 8 shows instantaneous visualisations of the flame predicted by the SDR closure and FSD models. In all cases, large pockets of unburned gases travel down the length of the combustion chamber in a puffing motion due to the sinusoidal pulsations added at the inlet in order to emulate the combustion instability. A series of flame visualisations, lasting for a full time period of $1/f_1 = 0.02s$, were shown in an earlier study (see Fig.7 of Ref. [28] and thus are not repeated here). The flame predicted by SDR generally yields a thinner flame brush, particularly in comparison to the FurebyM model. One possible reason is that the filtered reaction rate using the SDR closure method is not a function of $|\nabla \tilde{c}|$, which, following Eq. (11) or the BML relation [8,66] for the present grid resolution, results in a larger value of FSD at the leading edge of the flame brush than towards the

burned gas side. This, in turn, leads to faster propagation speed at the leading edge of the flame brush than at the trailing edge [28]. The difference in propagation speeds between the leading and trailing edges of the flame brush for the models with $|\nabla \bar{c}|$ dependence (e.g. FurebyM model) leads to flame thickening for the FurebyM model. However, the sub-grid CGT modelling may reduce the rate of flame thickening. Another possible reason for the thinner flame brush predicted by the SDR closure is that the magnitude of $|\nabla \bar{c}|$ or $|\nabla \tilde{c}|$ for the FurebyM and Muppala models remains small close to $\tilde{c} = 1$ of the flame brush, so partially burned gases are consumed at a slower rate. Furthermore, slower burning is encountered in locally homogeneous distributions of $\bar{c}$ or $\tilde{c}$ due to negligible contribution of the chemical source term. By contrast, $\tilde{c}(1-\tilde{c})$ within the SDR $\tilde{N}_c$ model given by Eq. (16) yields non-negligible chemical reaction even in locally homogeneous pockets of $\tilde{c}$ for $0 < \tilde{c} < 1.0$.

Figure 9 shows the mean and fluctuating velocities predicted by the three models, where the mean velocity is calculated by taking the time average of the Favre filtered velocity and the fluctuating velocity is evaluated from the resolved variance. It has been found in a previous analysis [28] that the wrinkling factor for the majority of FSD models are not much greater than unity when a grid resolution of 2mm is applied for the two test cases which are studied here. This suggests that most of the flame surface area is resolved. Furthermore, the grid sensitivity study for the SDR model shows minor quantitative changes in the velocity fluctuations for the two grid resolutions. For these reasons, it is believed that the resolved variance of velocity components sufficiently represent the fluctuating velocity components [28]. The velocity predictions of the SDR method are

comparable to those of the FurebyM and Muppala models, yielding a satisfactory agreement with experimental measurements. However, it can be observed that the SDR method is able to capture the experimental mean and fluctuating axial velocities qualitatively better in regions towards the walls of the combustor. This may be attributed to the prediction of a thinner flame brush that enables the smaller resolved eddies to corrugate the flame, producing a relatively larger observed radius of negative flame curvature near the walls. The effects of thinner flame brush in case of SDR based closure can further be seen in the mean transverse velocity profiles, where the peaks corresponding to the maximum values are drawn slightly closer towards the central axis in span-wise direction. Like the results obtained from FSD based formulations, over-predictions in the transverse mean velocities are also observed for the SDR based closure. These over-predictions can be attributed partially due to the effects of combustion instability, which may not have been fully emulated in the transverse direction.

In terms of the transverse velocity fluctuations, the SDR based closure is able to capture the peaks at x/h = 2 and predictions are expected to improve with finer grids for the upstream location at x/h = 1. The FurebyM model seemingly captures these higher transverse velocity fluctuations at x/h = 1. Further downstream, the velocity fluctuations predicted by the SDR based formulation are found to be comparable to the FSD models (i.e FurebyM and Muppala models) considered here.

4.3.2. Volvo Rig

Instantaneous flame visualisations predicted by SDR and FSD models are shown in Fig. 10. A series of instantaneous flame visualisations (not shown here) for the SDR based

closure display more symmetrical pulsing of the burned gases rather than asymmetric flame propagation, leading to disconnected regions of homogeneously burned gases. However a higher value of β_c than 3.3 leads to an asymmetric flame shape similar to that obtained for the FSD based closures. Lower values of β_c may cause higher reaction rates, leading to higher temperature-dependent viscosities which dampen out the asymmetric shedding of vortices from the flame holder. This may result in the loss of the asymmetric flame shape for low β_c values. To the authors' knowledge, symmetrical vortex shedding or symmetrical flame propagation was observed experimentally with high-speed video photography and flash Schlieren imaging [28] for the operating condition of $U_0 = 17.3\,\text{m/s}$ and $T = 273K$, and this behaviour was also predicted in LES [81,94]. For the current operating conditions (i.e. $U_0 = 37.0\,\text{m/s}$ and $T = 600K$), asymmetric flame propagation (Karman vortex street) was predicted by other LES studies [81,82] and the two FSD models exhibit similar sinusoidal-like behaviour. There is no strong case to suggest that the symmetrical pulsing behaviour is not realistic, but it is important to stress that a change in the predicted behaviour can be brought about by a small change in the value of β_c. Similar to the ORACLES burner, the SDR method predicts a thinner flame brush. From Fig. 10, it can also be deduced that the FurebyM model will yield the lowest mean temperatures because of the segmented regions of partially burned gases. By contrast, the Muppala and SDR models are expected to deliver higher levels of heat release throughout the combustor due to a greater proportion of homogeneously burned gases.

The mean and fluctuating velocity plots comparing SDR and FSD models are shown in Fig. 11 and all three models generally yield a satisfactory agreement with experiments. The observed differences in flame propagation for the SDR approach are reflected in these plots by the greater axial flow acceleration at *x/H* = 9.40 and the different qualitative trends of the velocity fluctuations. The presence of wider and more rectangular regions of the burned gases downstream of the combustor point to greater levels of heat release and increased uniformity of the u'/U_0 profiles at *x/H* = 3.75 and 9.40. In the transverse direction, the predicted mean velocities of the SDR approach are similar to those of the FurebyM and Muppala models, whereas the fluctuations are generally under-predicted, possibly arising from the reduced levels of asymmetric flame propagation.

The temperature plots in Fig. 12 reveal more clearly the potential advantages of applying the SDR closure. The mean temperatures are significantly better captured both quantitatively and qualitatively by the SDR based closure than by the FSD based formulations. The FurebyM model yields insufficient levels of heat release whereas the Muppala model under-predicts the mean flame spread T/T_{ad} at *x/H* = 9.40. In terms of temperature fluctuations however, the SDR based closure over-predicts the magnitude at *x/H* = 3.75, corresponding to the observed pulsating nature of the predicted flame. The FSD closures based on the FurebyM and Muppala models yield similar quantitative predictions.

5. CONCLUSIONS

The performance of a newly developed reaction rate closure based on algebraic modelling of SDR $\tilde{N}_c$ model has been assessed based on simultaneous *a-priori* DNS analysis and *a-posteriori* LES analyses. A simple chemistry DNS database of statistically planar turbulent premixed flames with global Lewis numbers Le ranging from 0.34 to 1.2 has been explicitly filtered using a Gaussian filter kernel for the purpose of *a-priori* analysis. The *a-posteriori* analysis has been conducted by the LES of turbulent premixed flames in two well-documented configurations, namely, the ORACLES burner and the Volvo Rig. It was found that an algebraic expression involving Favre filtered SDR $\tilde{N}_c$, which was originally proposed in the context of RANS, can be used to model the filtered reaction rate $\overline{\dot{w}}$ for filter widths greater than the thermal flame thickness (i.e. $\Delta > \delta_{th}$). An existing algebraic closure of SDR for RANS has been extended here for the purpose of LES, and the optimum value of the model parameter β_c has been calibrated in such a manner that the variation of the volume averaged wrinkling factor $\Xi_D^V = \left\{\bar{\rho}\tilde{N}_c\right\}_V \Big/ \left\{\bar{\rho}\tilde{D}\nabla\tilde{c}\cdot\nabla\tilde{c}\right\}_V$ with changing Δ/δ_{th} is accurately captured. This proposed algebraic SDR model satisfactorily captures the quantitative variation of $\tilde{N}_c$ with $\tilde{c}$ throughout the flame brush for a range of different filter widths and the optimum value of β_c is found to be dependent on the modelling of sub-grid scale velocity fluctuation u'_Δ. The newly developed SDR based reaction rate closure was then implemented for LES of the ORACLES burner and the Volvo Rig and its performance was compared against two different algebraic FSD closures [56,59] that performed relatively well in a previous analysis [28]. The SDR based closure generally predicts a thinner resolved flame brush with a performance that either is comparable to or better than the FSD based closures

considered here. For the ORACLES burner, the qualitative trend of the mean and fluctuating axial velocities near the walls are better captured by the SDR method than by the FSD based closures. Greater differences between the predictions of the SDR and FSD approaches are observed for the Volvo Rig. The former method predicts a flame that seemingly pulsates particularly for small values of β_c, leaving behind disconnected regions of the burned gas. By contrast, the FurebyM and Muppala models yield a flame that propagates asymmetrically. The pulsating behaviour of the flame predicted by the SDR method generates higher fluctuations in the axial velocity and temperature, but the corresponding mean quantities are better predicted than the FSD based closures. This is particularly the case for the mean temperature profiles, where the width and mean temperature of the flame are well captured by the newly developed SDR based closure. The satisfactory predictions of the newly developed SDR based closure for the both test cases indicate that this methodology has the potential to be a viable option for LES simulations of turbulent premixed combustion.

It is worth noting that the *a-priori* analysis in this work has been carried out for simple chemistry DNS data with moderate values of turbulent Reynolds number Re_t and therefore further analysis based on three-dimensional DNS data with higher values of Re_t is necessary for a more comprehensive analysis. Moreover, future work will require looking into the sensitivity of the input parameters to the performance of the SDR model. For example, preliminary runs have shown that different values of β_c can significantly affect the predicted LES results. It is perhaps possible to improve the prediction of the SDR model by dynamic evaluation of β_c, which will remove the empiricism involved in

the parameterisation given by Eq. (19). The LES closure of SDR using a dynamic evaluation of β_c is beyond the scope of the present analysis and will be addressed in future work. The SDR model should also be tested for a range of different premixed combustion regimes in order to assess the range of its applicability.

ACKNOWLEDGEMENTS

We are grateful to the UK Engineering and Physical Sciences Research Council (EPSRC) for financial assistance.

Appendix A. Physical basis of the algebraic SDR model

The original RANS model by Kolla *et al.* [18] takes the following form:

$$\breve{\varepsilon}_c = \left[2K_c^* \frac{S_L}{\delta_{th}} + (C_3' - \tau C_4' Da_L) \frac{\breve{\varepsilon}}{\breve{k}} \right] \frac{\breve{c}(1-\breve{c})}{\beta_1'} \tag{A1}$$

$$\text{with} \quad C_3' = \frac{1.5\sqrt{Ka_L}}{(1+\sqrt{Ka_L})}; \; C_4' = \frac{1.1}{(1+Ka_L)^{0.4}} \quad \text{and} \quad \beta_1' = 6.7 \tag{A2}$$

In Eq. (A1) $\breve{k} = <\rho u_i'' u_i''> / <\rho>$, $\breve{\varepsilon} = <\mu(\partial u_i''/\partial x_j)(\partial u_i''/\partial x_j)> / <\rho>$ and $Da_L = \breve{k} S_L / \breve{\varepsilon}\delta_{th}$ are the turbulent kinetic energy, its dissipation rate and local Damköhler number respectively, whereas $Ka_L = (\breve{\varepsilon}\delta_{th})^{1/2} S_L^{-3/2}$ is the local Karlovitz number. Equation (A1) has been derived based on the equilibrium of the leading order terms in the $\breve{\varepsilon}$ transport equation (i.e. $I + II + III + IV \approx 0.0$) where the terms I, II, III and IV are given by [6,15,19,21]:

$$I = -\left\langle 2D \frac{[\dot{w} + \nabla.(\rho D \nabla c)]}{\rho} \frac{\partial c}{\partial x_k} \frac{\partial \rho}{\partial x_k} \right\rangle + 2 \frac{\langle D \rangle}{\langle \rho \rangle} \frac{\partial \breve{c}}{\partial x_k} \frac{\partial \langle \rho \rangle}{\partial x_k} \left[\langle \dot{w} + \nabla.(\rho D \nabla c) \rangle - \frac{\partial \langle \rho u_j'' c'' \rangle}{\partial x_j} \right] \tag{A3}$$

$$II = -2\left\langle \rho D \frac{\partial c''}{\partial x_i} \frac{\partial u_i''}{\partial x_j} \frac{\partial c''}{\partial x_j} \right\rangle \tag{A4}$$

$$III = \left\langle 2D \frac{\partial \dot{w}}{\partial x_k} \frac{\partial c}{\partial x_k} \right\rangle - 2\langle D \rangle \frac{\partial \langle \dot{w} \rangle}{\partial x_k} \frac{\partial \breve{c}}{\partial x_k} \tag{A5}$$

$$IV = -2\left\langle \rho D^2 \frac{\partial^2 c''}{\partial x_i \partial x_j} \frac{\partial^2 c''}{\partial x_i \partial x_j} \right\rangle \tag{A6}$$

For low Mach number, globally adiabatic, unity Lewis number flames the term II can be simplified as: $II \approx <2\rho \nabla . \vec{u} \varepsilon_c >$ [14,15,19,21] so this term can be modelled as: $II = 2K_c^*(S_L / \delta_{th}) < \rho > \breve{\varepsilon}_c$ using the definition of K_c^* (see Eq. (14i)). The terms $< \rho > (C_3' - \tau C_4' Da_L)(\breve{\varepsilon} / \breve{k}) \breve{\varepsilon}_c$ and $- < \rho > \beta_1' \breve{\varepsilon}_c^2 / [\breve{c}(1 - \breve{c})]$ are the modelled expressions for II and $(III + IV)$ respectively [15,19,21]. Thus, $(I + II + III + IV) \approx 0.0$ leads to Eq. (A1). It is worth noting $< \rho > C_3'(\breve{\varepsilon} / \breve{k}) \breve{\varepsilon}_c$ accounts for the generation of SDR arising from the term II due to the alignment of ∇c with the most compressive principal strain rate, whereas $- < \rho > \tau C_4' Da_L (\breve{\varepsilon} / \breve{k}) \breve{\varepsilon}_c$ models the destruction of SDR due to the alignment of ∇c with the most extensive principal strain rate under the action of flame normal acceleration. The effects of flame normal acceleration weaken with increasing Karlovitz number which is accounted for by Ka_Δ (Ka_L) dependence of C_4 (C_4') in Eq. (13i) (Eq. (A1)). It is possible to obtain an expression for turbulent flame speed $S_T = 2\sqrt{(D_t / \rho_0)(\partial < \dot{w} > / \partial \breve{c})_{\breve{c}=0}}$ according to Kolmogorov-Petrovsky-Piskunov (KPP) theorem using Eqs. (1) and (A1) [18]. It has been shown in Ref. [18] that the algebraic SDR model given by Eq. (A1) enables satisfactory prediction of turbulent flame speed for a number of different experimental configurations. Moreover, Eq. (A1) has been

successfully implemented in RANS simulations which yielded good agreement with experimental results [22-24]. Interested readers are referred to Kolla *et al.* [18] for further information regarding the validation of the algebraic SDR model given by Eq. (A1).

A comparison between Eqs. (13ii) and (A2) reveals that the expressions for C_3 and C_4 are directly extended from C_3' and C_4' respectively [18], and the value of β_1 has been modified in comparison to β_1' for the purpose of extending Eq. (A1) for LES. Chakraborty and Swaminathan [20] modified the model by Kolla *et al*. [18] for non-unity Lewis number flames in the following manner:

$$\breve{\varepsilon}_c = \left[2K_c^* \frac{S_L}{Le^{1.88}\delta_{th}} + (C_3'^* - \tau C_4'^* Da_L) \frac{\breve{\varepsilon}}{\breve{k}} \right] \frac{\breve{c}(1-\breve{c})}{\beta_c'} \qquad \text{(A7)}$$

with $C_3'^* = \dfrac{2.0\sqrt{Ka_L}}{(1+\sqrt{Ka_L})}$, $C_4'^* = \dfrac{1.2(1.0-c)^{b'}}{Le^{2.57}(1+Ka_L)^{0.4}}$, $b' = 0.2 + 1.5|1.0 - Le|$ and $\beta_1' = 6.7$ (A8)

Equation (A7) is similar to Eq. (A1) but the strengthening of density gradient magnitude and flame normal acceleration are addressed by $2K_c^* S_L/(Le^{1.88}\delta_{th})$ and Le dependence of $C_4'^*$ respectively. For $Le = 1.0$ flames Eqs. (A7) and (A1) provide comparable predictions [20].

APPENDIX B. Sensitivity study of grid resolution for SDR based closure

The application of a finer grid of 1mm generally yields noticeable improvements for the two test configurations in the context of SDR based closure. This is contrary to the findings based on algebraic FSD models, as reported in an earlier analysis [28], where mean velocities for the ORACLES burner were largely over-predicted for the FurebyM

model. The following discussion is based on the predictions of the SDR based closure, though the results of the FSD models (FurebyM and Muppala) for both grid resolutions are also presented in Figs. 13-15 for the reader's reference. For the ORACLES burner, there is a marked reduction in flow acceleration in both stream-wise and transverse directions (Fig. 13), leading to a closer agreement with experimental data. The velocity fluctuations, in particular, are better captured near the walls of the combustor. For the Volvo Rig, a series of instantaneous flame images (not shown here) show that the symmetrical pulsing behavior of the flame is less apparent and the higher predictions of the velocity (Fig. 14) and temperature fluctuations (Fig. 15) near the shear layers at x/H = 0.95 originate due to the improved resolution of smaller turbulent structures. The burned gas regions behind the flame holder are also less segmented, leading to the lower fluctuations in the central span-wise regions of the combustor downstream. By contrast, minor improvements are observed for the predicted mean velocities and temperature with grid refinement.

APPENDIX C. Sensitivity study of model parameter β_c

The *a-priori* analysis in Section 3.2 has indicated that the optimum values of β_c in Eq. (16) are 4.6 and 3.3 for $\tau = 6.17$ and $\tau = 2.13$ respectively, when u'_{Δ} is evaluated using the Smagorinsky model. However, in an actual LES, the modelling and numerical uncertainties may influence the optimum β_c value and the level of accuracy of the Smagorinsky model may not be consistent for the two test configurations considered here. Furthermore, the optimum value of β_c has been parameterised based on limited

number of cases. Thus, it is useful to carry out a sensitivity analysis based on the variation of β_c values for both the test configurations considered here.

By employing $\beta_c = 3.7$ for the ORACLES burner, mean velocities are over-predicted, particularly near the combustor walls as shown in Fig. 16. By contrast, $\beta_c = 4.6$ and $\beta_c = 5.2$ yield a satisfactory agreement with experiments. A series of instantaneous flame visualisations (not shown here) reveals a reduced volume of the unburned gas reaching the walls of the combustor, indicating the presence of higher reaction rates and therefore greater flow acceleration. An inspection of Eq. (16) further suggests that the use of a smaller value of β_c results in higher reaction rates. Similarly, greater mean temperatures are observed in Fig. 17 for the Volvo Rig when β_c is reduced, though a better agreement with experimental data is attained for $\beta = 3.3 (<4.6)$ due to the difference in the global heat release parameter. Unlike the ORACLES burner however, greater differences in flame shape were observed in VOLVO Rig when the model parameter is altered. As β_c is reduced, symmetrical pulsing (instead of asymmetric pulsing) occurs behind the flame holder leading to disconnected regions of the burned gas. The pulsing leads to the higher velocity (Fig. 18) and temperature fluctuations (Fig. 17) near the shear layers at x/H = 0.95, and the higher values in the central span-wise regions at x/H = 3.75 originate partially due to the segmented regions of the burned gas. This pulsing behavior may arise from the higher reaction rates which produce higher temperature-dependent viscosities that dampen the asymmetric shedding of vortices behind the flame holder. Based on this reasoning, at an even lower β_c value of 2.2, the

dampening effect increases and so the degree of vertical flame corrugation reduces. Figure 17 therefore shows a noticeable drop in temperature fluctuations (from $\beta_c = 3.3$ to 2.2) at the central span-wise regions of x/H=3.75 and x/H = 9.40 with a 10% increase in the maximum mean temperature. Overall, $\beta_c = 3.3$ satisfactorily captures the mean experimental data both quantitatively and qualitatively. Moreover, $\beta_c = 3.3$ in this case is consistent with the prediction of Eq. (19) which is obtained based on *a-priori* analysis of DNS data.

REFERENCES

[1] N. Peters, Turbulent Combustion, Cambridge University Press (2000).

[2] D. Veynante, T. Poinsot, Large Eddy Simulations of combustion instabilities in turbulent premixed burners, *Annual Research Briefs 1997*, Centre for Turbulence Research, Stanford University, USA, pp.253-275 (1997).

[3] O. Colin, F. Ducros, D. Veynante, T. Poinsot, *Phys. Fluids.* 12 (2000) 1843-1863

[4] S.M. Candel, T. J. Poinsot, *Combust. Sci. Technol.*, **70** (1990) 1-15.

[5] D. Veynante, L. Vervisch, *Prog. Energy and Combust. Sci*., 28 (2002) 193-266 (2002).

[6] N. Chakraborty, M. Champion, A. Mura, N. Swaminathan, "Scalar dissipation rate approach to reaction rate closure", Turbulent premixed flame, (Eds. N. Swaminathan, K.N.C. Bray), Cambridge University Press, 1st Edition, Cambridge, UK, pp. 74-102, 2011.

[7] R.W. Bilger, *Flow Turb. Combust*. 72 (2004) 93-114.

[8] K.N.C. Bray, *Turbulent Reacting Flows*, Springer Verlag, Berlin, Heidelburg, New York, eds. P.A.Libby and F.A. Williams (1980) 115-183.

[9] N. Chakraborty, R.S. Cant, *Combust. Flame*, 158 (2011) 1768-1787.

[10] R. Borghi and D. Dutoya, *Proc. Combust. Inst.* 17 (1978) 235-244.

[11] R. Borghi, *Combust. Flame*, 80 (1990) 304-312.

[12] T. Mantel and R. Borghi, *Combust. Flame*, 96 (1994) 443-457.

[13] A. Mura and R. Borghi, *Combust. Flame*, 133 (2003) 193-196.

[14] N. Swaminathan and K. N.C. Bray, *Combust. Flame*, 143 (2005) 549-565.

[15] N. Chakraborty, J.W. Rogerson, N. Swaminathan, *Phys. Fluids* ,20 (2008) 045106.

[16] A. Mura, K. Tsuboi and T. Hasegawa, *Combust. Theory Modell.*, 12 (4) (2008) 671-698.

[17] A. Mura, V. Robin, M. Champion, T. Hasegawa, *Flow Turb. Combust*., 82 (2009) 339-358.

[18] H. Kolla, J. Rogerson, N. Chakraborty, N. Swaminathan, *Combust. Sci. Technol.*, 181 (2009) 518-535, 2009.

[19] N. Chakraborty, J. Rogerson, N. Swaminathan, *Flow Turb. Combust.*, 85 (2010) 25-55.

[20] N. Chakraborty, N. Swaminathan, *Flow Turb. Combust.*, 87 (2011) 261-292.

[21] N. Chakraborty, N. Swaminathan, *Combust. Sci. Technol.*, 185 (2013) 676-709.

[22] H. Kolla, N., Swaminathan, *Combust. Flame*, 157 (2010) 943-954.

[23] S. Sadasivuni, G. Bulat, V. Senderson, N. Swaminathan, Paper no. GT2012-68483, Proc. of ASME TURBO EXPO 2012: Power for Land, Sea and Air GT2012, June 11-15, 2012, Bella Center, Copenhagen, Denmark (2012)

[24] I. Ahmed, N. Swaminathan, *Combust. Sci. Technol.* 185(10) (2013) 1509-1540.

[25] T. Dunstan, Y. Minamoto, N. Chakraborty, N. Swaminathan, *Proc. Comb. Inst*. 34 (2013) 1193-1201.

[26] Y. Gao, N. Chakraborty, N. Swaminathan, Algebraic closure of scalar dissipation rate for Large Eddy Simulations of turbulent premixed combustion, 24th International Colloquium on Dynamics of Explosions and Reactive Systems, Taiwan, 2013.

[27] P. Nguyen, P. Bruel, and S. Reichstadt, *Flow, Turb. Combust*., 82 (2009) 155–183.

[28] T. Ma, O. Stein, N. Chakraborty, A. Kempf, *Combust. Theor. Modell.* 17(3) (2013) 431-482.

[29] A. Sjunnesson, P. Henrikson, C. Löfström, *AIAA*, 28 (1992), 92-3650.

[30] C. Fureby, S.I. Möller, *AIAA*, 33 (1995), 2339-2347.

[31] M. Boger, D. Veynante, H. Boughanem, A. Trouvé, *Proc. Combust. Inst*., 27, 917–925 (1998).

[32] N. Chakraborty, M. Klein, *Phys. Fluids*, 20 (2008) 085108.

[33] M. Katragadda, N. Chakraborty, R.S. Cant, *J. Combust.* (2012) 353257.

[34] M. Katragadda, N. Chakraborty, R.S. Cant, *J. Combust.* (2012) 794671.

[35] J.B. Moss, *Combust. Sci. Technol*, 22(1980)119-129.

[36] I.G. Shepherd, J. B. Moss and K. N.C. Bray, *Proc. Combust. Inst.*, 19 (1982) 423-431.

[37] R. K. Cheng, I. G. Shepherd, *Combust. Flame*, 85 (1991)7-26.

[38] N.W. H. Armstrong, K. N. C. Bray, *Proc. SAE*, 922322 (1992).

[39] C.J. Rutland, R. S. Cant, Proc. of summer program, Stanford, CA, 1994, Centre for Turbulence Research, NASA Ames/ Stanford University (1994).

[40] D. Veynante, A. Trouvé, K.N.C. Bray, T. Mantel, *J. Fluid Mech*., 332 (1997) 263-293.

[41] D. Veynante and T. J. Poinsot, *J. Fluid Mech*., 353(1997) 83-114.

[42] H.G. Weller, G. Tabor, A.D. Gosman and C. Fureby, *Proc. Combust. Inst*., 27 (1998) 899–907.

[43] J.H. Frank, P.A. M. Kalt, R.W. Bilger, *Combust. Flame*, 116 (1999) 220-232.

[44] M. Boger, Sub-grid scale modeling for large eddy simulation of turbulent premixed combustion, PhD dissertation, E´ cole Centrale Paris (2000).

[45] N. Swaminathan, R.W. Bilger, B. Cuenot, *Combust. Flame*, 126(2001)1764-1779.

[46] P.A.M. Kalt, Y.C. Chen, R.W. Bilger, *Combust. Flame*, 129 (4) (2002) 401-415.

[47] S.W. Tullis and R.S. Cant, *Proc. Combust. Inst*., 29 (2003) 2097-2104.

[48] S. Nishiki, T. Hasegawa, R. Borghi, R. Himeno, *Combust. Theory Modelling*, 10 (2006) 39-55.

[49] N. Chakraborty, R.S. Cant, *Phys. Fluids.*, 21 (2009) 035110.

[50] N. Chakraborty, R.S. Cant, *Combust. Flame,* 156 (2009)1427-1444.

[51] N. Chakraborty, R.S. Cant, *Num. Heat Trans. A*, 55 (2009) 762-779.

[52] G. Lecocq, S. Richard, O. Colin, L. Vervisch, *Combust. Sci. Technol.*, 182 (2010) 465-479.

[53] S. Pfadler F. Dinkelacker, F. Beyrau, A. Leipertz, *Combust. Flame,* 156 (2009) 1552-1564.

[54] S. Pfadler, J. Kerl, F. Beyrau, A. Leipertz, A. Sadiki, J. Scheuerlein, F. Dinkelacker, *Proc. Combust. Inst.*, 32 (2009) 1723-1730.

[55] W. Meier, P. Weigand, X.R. Duan and R. Giezendanner-Thoben, *Combust. Flame*, 150 (2007) 2–26.

[56] S. Muppala, N. Aluri, F. Dinkelacker, and A. Leipertz, Combust. Flame 140 (2005) 257–266.

[57] M. Düsing, Large-Eddy Simulation turbulenter Vormischflammen, Technische Universität Darmstadt, 2004.

[58] P. Wang and X. Bai, Large eddy simulation of turbulent premixed flames using level-set G-equation, *Proc. Combust. Inst*., 30 (2005) 583–591.

[59] C. Fureby, *Proc. Combust. Inst*., 30 (2005) 593–601.

[60] W. Sutherland, *Phil. Mag*., 36 (1893), 507.

[61] S. Richard, O. Colin, O. Vermorel, C. Angelberger, A. Benkenida, and D. Veynante, *Proc. Combust. Inst*., 31 (2007) 3059–3066.

[62] J. Smagorinsky, Monthly Weather Review 91 (1963), pp. 99–164

[63] N. Aluri, S. Muppala, and F. Dinkelacker, *Flow, Turb. Combust*., 80 (2008)207–224.

[64] B. Manickam, J. Franke, S.P.R. Muppala, and F. Dinkelacker, LES of Triangular-stabilized Lean Premixed Turbulent Flames with an algebraic reaction closure: Quality and Error Assessment, in Quality and Reliability of Large-Eddy Simulations II, , M.V. Salvetti, B. Geurts, J. Meyers, eds., Springer Netherlands, 2011, pp. 221–230.

[65] N. Chakraborty, R. Cant, *Phys. Fluids,* 19 (2007) 105101.

[66] K.N.C. Bray, P.A. Libby and J.B. Moss, *Combust. Flame* 61 (1985) 87-102.

[67] J.W. Rogerson, N. Swaminathan, Correlation between dilatation and scalar dissipation in turbulent premixed flames, *Proc. 3rd European Combustion Meeting* Crete, Chaina, Greece, 11th to 13th April, 2007.

[68] T. Poinsot and D. Veynante, *Theoretical and numerical combustion*, R.T.Edwards Inc., Philadelphia, USA (2001).

[69] N. Chakraborty, M. Katragadda, R.S. Cant, *Phys. Fluids*, 23 (2011) 075109.

[70] N. Chakraborty, M. Katragadda, R.S. Cant, *Flow Turb. Combust.*, 87 (2011) 205-235.

[71] C. Jiménez, B. Cuenot, T. Poinsot, D. Haworth, *Combust. Flame,* 128 (2002) 1-21.

[72] F.Charlette, C.Meneveau, D.Veynante, *Combust. Flame*, 131 (2002) 159-180.

[73] N. Swaminathan, R.W. Grout, *Phys. Fluids.* 18 (2006) 045102.

[74] R.W. Grout, *Phys. Fluids*, 19 (2007)105107.

[75] I. Han, K.H. Huh, *Combust. Flame*, 152 (2008) 194-205.

[76] I. Han, K.H. Huh, *Proc. Combust. Inst*., 32 (2009) 1419-1425.

[77] M. Besson, P. Bruel, J.L. Champion, B. Deshaies, *J. Thermophys. Heat Transfer*, 14(1) (2000) 59-68

[78] T. Broeckhoven, M. Freitag, C. Lacor, A. Sadiki, J. Janicka, *Complex Effects in Large Eddy Simulations*, (2007) 353-369.

[79] P. Domingo, L. Vervisch, S. Payet, R. Hauguel, *Combust. Flame*, 143 (2005), 566-586.

[80] C. Duwig, C. Fureby, *Combust. Flame*, 151 (2007), 85-103.

[81] E. Baudoin, R. Yu, K.J. Nogenmyr, X.S. Bai, C. Fureby, *AIAA*, (2009), 1178

[82] C. Fureby, *Combust. Sci. Tech.*, 161 (2000), 213-243.

[83] B. Manickam, J. Franke, S.P.R. Muppala, F. Dinkelacker, *Flow Turb. Combust.*, 88 (2012), 563-596.

[84] A. Sjunnesson, C. Nelsson, E. Max, *Laser Anemometry*, 3 (1991), 83-90.

[85] F. Cavallo Marincola, T. Ma, A.M. Kempf, *Proc. Combust. Inst.*, 34 (2013), 1307-1315.

[86] C. Olbricht, O. Stein, J. Janicka, J. van Oijen, S. Wysocki, A. Kempf, *Fuel*, 96 (2012), 100-107.

[87] M. Pettit, B. Coriton, A. Gomez, A. Kempf, *Proc. Combust. Inst.*, 33 (2011), 1391-1399.

[88] O. Stein, B. Böhm, A. Dreizler, A. Kempf, *Flow Turb. Combust.* 87 (2010), 425-447.

[89] A. Kempf, *TU Darmstadt*, Germany, 2003.

[90] R. Keppeler, M. Pfitzner, L.T.W. Chong, T. Komarek, W. Polifke, *ASME Conf. Proc.*, GT2012-68689 (2012).

[91] M. Klein, A. Sadiki, J. Janicka, *J. Comput. Phys.*, 186 (2003), 652-665.

[92] A. Kempf, M. Klein, J. Janicka, *Flow Turb. Combust.*, 74 (2005), 67-84.

[93] M. Germano, U. Piomelli, P. Moin, W.H. Cabot. *Phys. Fluids*., 3(7), 1991, 1760-1765.

[94] S.I. Moller, E. Lundgren, C. Fureby. *Proc. Combust. Inst*., 26 (1996) 241-248.

TABLES

Modelling approach		Relevant equations
FurebyM [28, 59]	Modelled transport equation of $\tilde{c}$	$\bar{\rho}\left[\frac{\partial \tilde{c}}{\partial t}+\tilde{u}_j\frac{\partial \tilde{c}}{\partial x_j}\right]=\underbrace{\rho_0 S_L \Xi\lvert\nabla \bar{c}\rvert}_{=\rho_0 S_L \Sigma_{gen}}-\frac{\partial}{\partial x_j}[\overline{\rho u_j c}-\bar{\rho}\tilde{u}_j\tilde{c}]$
	Modelling of wrinkling factor Ξ	$\Xi=\left(1+\Gamma\frac{u'_\Delta}{S_L}\right)^{D_f-2}$ where $\Gamma=0.75\exp\left[-1.2\left(\frac{u'_\Delta}{S_L}\right)^{-0.3}\right]\left(\frac{\Delta}{\delta_z}\right)^{2/3}$ and $D_f=\frac{2.05}{u'_\Delta/S_L+1}+\frac{2.35}{S_L/u'_\Delta+1}$
	Model of sub-grid flux	$[\overline{\rho u_i c}-\bar{\rho}\tilde{u}_i\tilde{c}]=-\bar{\rho}D_t\frac{\partial \tilde{c}}{\partial x_i}-\rho_0 S_L(\bar{c}-\tilde{c})M_i$
Muppala [56]	Modelled transport equation of $\tilde{c}$	$\bar{\rho}\left[\frac{\partial \tilde{c}}{\partial t}+\tilde{u}_j\frac{\partial \tilde{c}}{\partial x_j}\right]=\frac{\partial}{\partial x_j}\left[\bar{\rho}(D_t+D)\frac{\partial \tilde{c}}{\partial x_j}\right]+\rho_0 S_L\Xi\lvert\nabla\tilde{c}\rvert$
	Modelling of wrinkling factor Ξ	$\Xi=1+\frac{0.46}{Le}\mathrm{Re}_\Delta^{0.25}\left(\frac{u'_\Delta}{S_L}\right)^{0.3}\left(\frac{\bar{p}}{p_0}\right)^{0.2}$ where $\mathrm{Re}_\Delta=u'_\Delta\Delta/\nu$
SDR	Modelled transport equation of $\tilde{c}$	$\bar{\rho}\left[\frac{\partial \tilde{c}}{\partial t}+\tilde{u}_j\frac{\partial \tilde{c}}{\partial x_j}\right]=\frac{\partial}{\partial x_j}\left[\bar{\rho}\tilde{D}\frac{\partial \tilde{c}}{\partial x_j}\right]+\frac{2\bar{\rho}\tilde{N}_c}{(2c_m-1)}-\frac{\partial}{\partial x_j}[\overline{\rho u_j c}-\bar{\rho}\tilde{u}_j\tilde{c}]$
	Model of Favre-filtered SDR $\tilde{N}_c$	$\tilde{N}_c=\tilde{D}\nabla\tilde{c}.\nabla\tilde{c}+(1-f_b)\left[\frac{2K_c^* S_L}{Le^{1.88}\delta_{th}}+(C_3^*-\tau Da_\Delta C_4^*)\frac{2u'_\Delta}{3\Delta}\right]\frac{\tilde{c}(1-\tilde{c})}{\beta_c}$ where $f_b=\exp[-0.7(\Delta/\delta_{th})^{1.7}]$; $C_3^*=2.0\sqrt{Ka_\Delta}/(1.0+\sqrt{Ka_\Delta})$; $C_4^*=1.2(1.0-\tilde{c})^b/[Le^{2.57}(1+Ka_\Delta)^{0.4}]$; $b=0.2+1.5\lvert 1.0-Le\rvert$; $Da_\Delta=\Delta S_L/u'_\Delta\delta_{th}$; $Ka_\Delta=(u'_\Delta/S_L)^{3/2}(\Delta/\delta_{th})^{-1/2}$
	Model of sub-grid flux	$[\overline{\rho u_i c}-\bar{\rho}\tilde{u}_i\tilde{c}]=-\bar{\rho}D_t\frac{\partial \tilde{c}}{\partial x_i}-\rho_0 S_L(\bar{c}-\tilde{c})M_i$

Table 1: Summary of the modelling methodologies adopted in this analysis.

Case	*Le*	u'/S_L	l/δ_{th}	τ	Re_t	*Da*	*Ka*
A	1.0	7.5	2.45	**3.0**	47.0	0.33	13.0
B	**0.34**	7.5	2.45	4.5	47.0	0.33	13.0
C	**0.6**	7.5	2.45	4.5	47.0	0.33	13.0
D	**0.8**	7.5	2.45	4.5	47.0	0.33	13.0
E	**1.0**	7.5	2.45	4.5	47.0	0.33	13.0
F	**1.2**	7.5	2.45	4.5	47.0	0.33	13.0

Table 2: Initial values of the simulation parameters and non-dimensional numbers relevant to the DNS database.

Re	U_0 (m/s)	ρ_0 (kg/m^3)	T_0 (K)	T_b (K)	ν_u (m^2/s)	S_L (m/s)	Φ
20,000	11.0	1.296	276	1980	1.66×10^{-5}	0.27	0.75

Table 3: Parameters used for the ORACLES burner LES.

Re	U_0 (m/s)	ρ_0 (kg/m^3)	T_0 (K)	T_b (K)	ν_u (m^2/s)	S_L (m/s)	Φ
28,000	37.0	0.591	600	1876	5.29×10^{-5}	0.76	0.58

Table 4: Parameters used for the Volvo Rig LES.

FIGURE CAPTIONS

Figure 1: Variation of mean values of the chemical source term $\overline{\dot{w}} \times \delta_{th} / \rho_0 S_L$ and its model $2\overline{\rho}\tilde{N}_c / (2c_m - 1) \times \delta_{th} / \rho_0 S_L$ conditional on $\tilde{c}$ across the flame brush for different filter widths for cases (a-f) A-F.

Figure 2: Variation of mean values of Da_D conditional on $\tilde{c}$ across the flame brush different filter widths for cases A-F.

Figure 3: Pdfs of c within the filter volume at $\tilde{c} = 0.5$ for different filter widths for cases (a-f) A-F.

Figure 4: Variations of the wrinkling factor $\Xi_D^V = \left\{\overline{\rho}\tilde{N}_c\right\}_V \Big/ \left\{\overline{\rho}\tilde{D}\nabla\tilde{c}\cdot\nabla\tilde{c}\right\}_V$ (——) with Δ / δ_{th} on a log-log plot along with the predictions of Eq. (16) with u'_Δ obtained from DNS and optimum values of β_c (i.e. $\beta_c = 3.3$ and 4.35 is used for cases A and B-F respectively) (○); u'_Δ evaluated using Eq. (10) and optimum values of β_c (i.e. $\beta_c = 2.86$ and 3.7 is used for cases A and B-F respectively) (□) and u'_Δ evaluated using Eq. (10) and and β_c is evaluated using Eq. (19) for cases A-F.

Figure 5: Variation of mean values of the normalised SDR $\tilde{N}_c \times \delta_{th} / S_L$ conditional on $\tilde{c}$ across the flame brush, for predictions of Eq. (16) with u'_Δ obtained from DNS and optimum values of β_c (i.e. $\beta_c = 3.3$ and 4.35 is used for cases A and B-F respectively); u'_Δ evaluated using Eq. (10) and optimum values of β_c (i.e. $\beta_c = 2.86$ and 3.7 is used for cases A and B-F respectively) and u'_Δ evaluated using Eq. (10) and β_c is evaluated using Eq. (19) at $\Delta \approx 0.8\delta_{th}$ (1st column) and $\Delta \approx 2.8\delta_{th}$ (2nd column) for cases A-F.

Figure 6: 2-D sketch of the ORACLES burner's combustion chamber, where h = 29.9mm. Interior width in the y-direction is 5.03h.

Figure 7: Sketch of the Volvo Rig's combustor, where H = 40mm. Interior width in the y-direction is 6H.

Figure 8: Instantaneous flame visualisations predicted by (a) SDR, (b) FurebyM and (c) Muppala models for the ORACLES burner.

Figure 9: Normalised mean and fluctuating velocities predicted by SDR, FurebyM and Muppala models for the ORACLES burner.

Figure 10: Instantaneous flame visualisations predicted by (a) SDR, (b) FurebyM and (c) Muppala models for the Volvo Rig.

Figure 11: Normalised mean and fluctuating velocities predicted by SDR, FurebyM and Muppala models for the Volvo Rig.

Figure 12: Normalised mean and fluctuating temperatures predicted by SDR, FurebyM and Muppala models for the Volvo Rig.

Figure 13: Normalised mean and fluctuating velocities predicted by the SDR based closure and FSD models using coarse and fine grids for the ORACLES burner.

Figure 14: Normalised mean and fluctuating velocities predicted by the SDR based closure and FSD models using coarse and fine grids for the Volvo Rig.

Figure 15: Normalised mean and fluctuating temperatures predicted by the SDR based closure and FSD models using coarse and fine grids for the Volvo Rig.

Figure 16: Normalised mean and fluctuating velocities predicted by $\beta_c = 3.7$, $\beta_c = 4.6$ and $\beta_c = 5.2$ at locations $x = 2h$, $x = 7h$ and $x = 9h$ for the ORACLES burner.

Figure 17: Normalised mean and fluctuating temperatures predicted by $\beta_c = 2.2$, $\beta_c = 3.3$ and $\beta_c = 5.0$ for the Volvo Rig.

Figure 18: Normalised mean and fluctuating velocities by $\beta_c = 2.2$, $\beta_c = 3.3$ and $\beta_c = 5.0$ for the Volvo Rig.

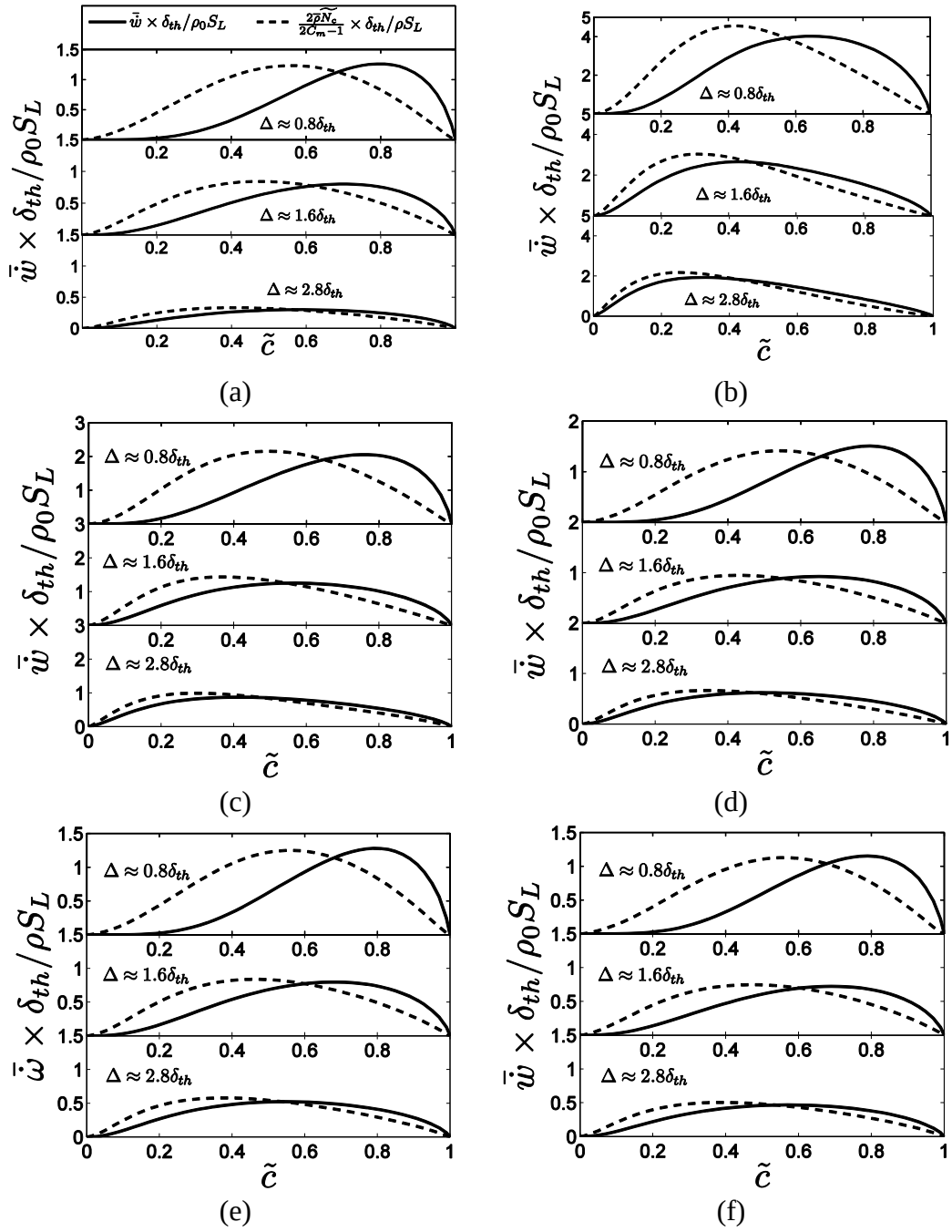

Figure 1: Variation of mean values of the chemical source term $\bar{\dot{w}} \times \delta_{th} / \rho_0 S_L$ and its model $2\bar{\rho}\widetilde{N}_c /(2c_m - 1) \times \delta_{th} / \rho_0 S_L$ conditional on $\tilde{c}$ across the flame brush for different filter widths for cases (a-f) A-F.

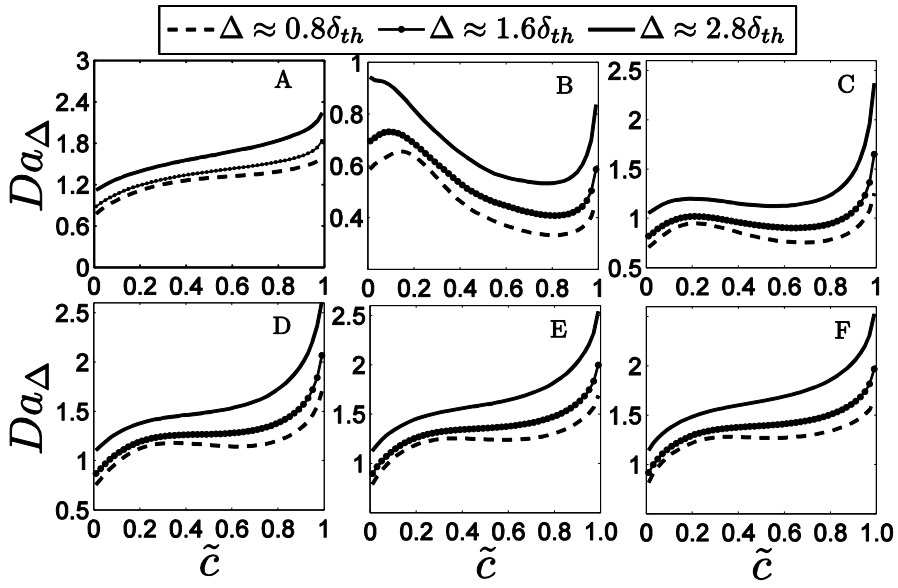

Figure 2: Variation of mean values of Da_Δ conditional on $\tilde{c}$ across the flame brush different filter widths for cases A-F.

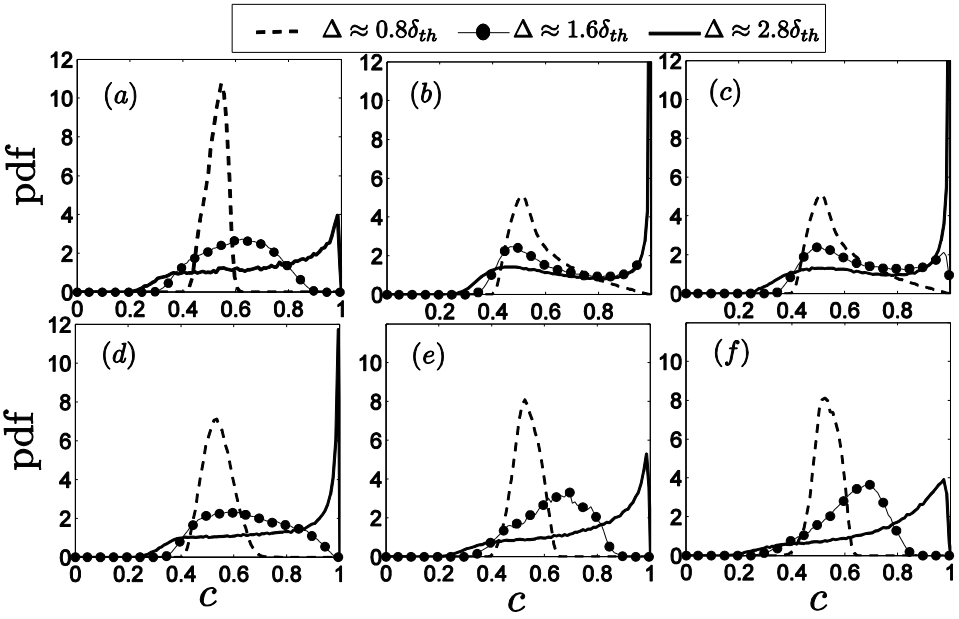

Figure 3: Pdfs of c within the filter volume at $\tilde{c} = 0.5$ for different filter widths for cases (a-f) A-F.

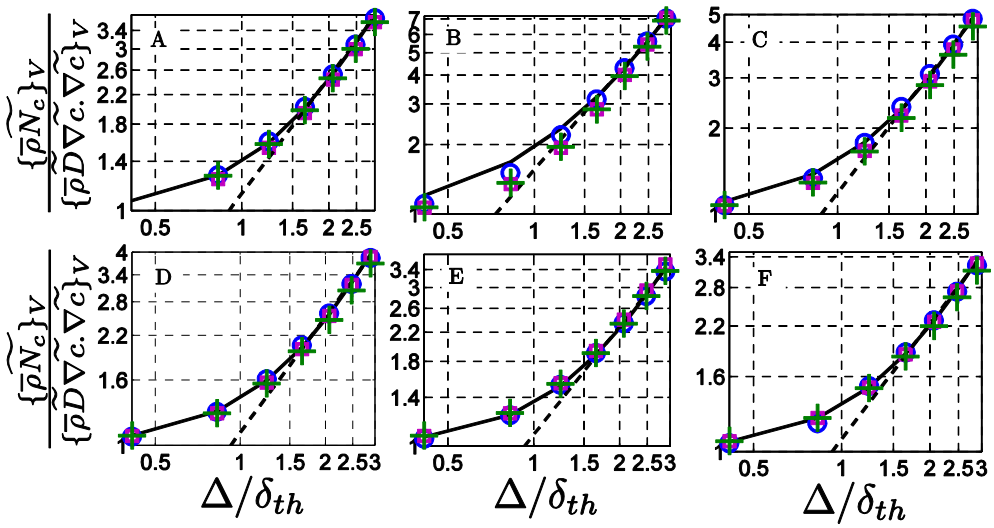

Figure 4: Variations of the wrinkling factor $\Xi_D^V = \left\{\bar{\rho}\tilde{N}_c\right\}_V \Big/ \left\{\bar{\rho}\tilde{D}\nabla\tilde{c}.\nabla\tilde{c}\right\}_V$ **(——) with** Δ/δ_{th} **on a log-log plot along with the predictions of Eq. (16) with** u'_Δ **obtained from DNS and optimum values of** β_c **(i.e.** $\beta_c = 3.3$ **and** 4.35 **is used for cases A and B-F respectively) (○);** u'_Δ **evaluated using Eq. (10) and optimum values of** β_c **(i.e.** $\beta_c = 2.86$ **and** 3.7 **is used for cases A and B-F respectively) (▫) and** u'_Δ **evaluated using Eq. (10) and** β_c **is evaluated using Eq. (19) for cases A-F (+).**

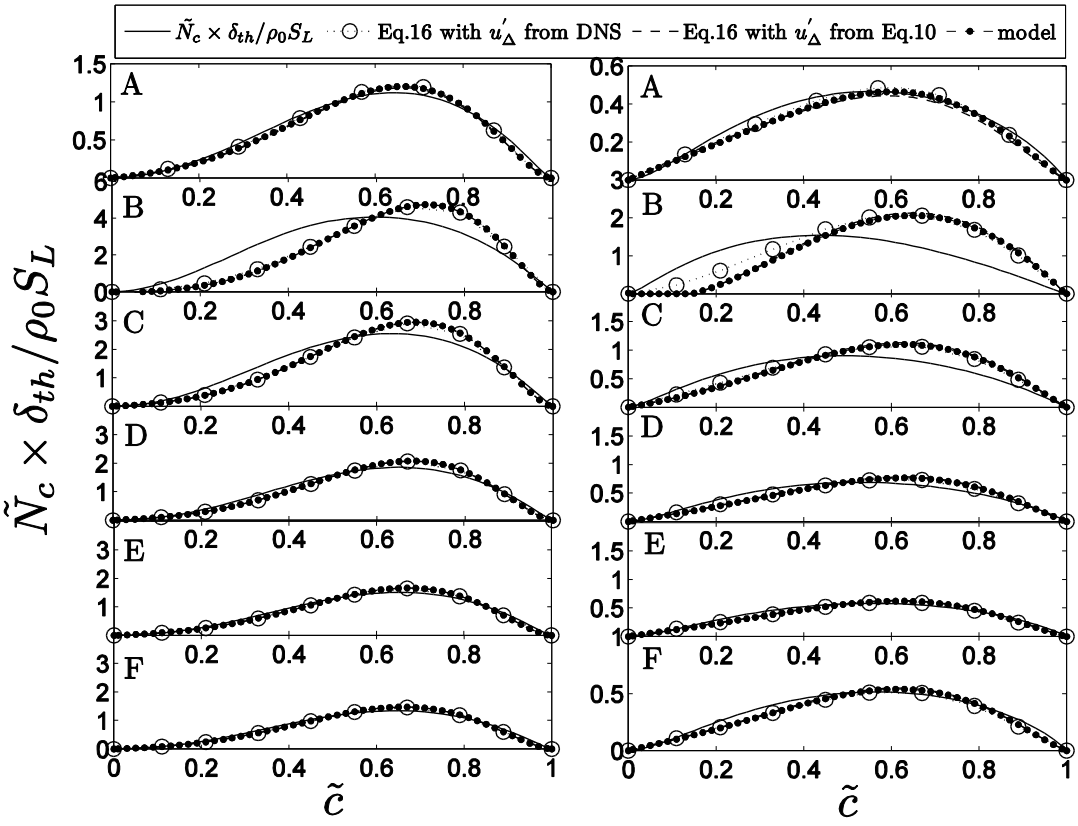

Figure 5: Variation of mean values of the normalised SDR $\tilde{N}_c \times \delta_{th} / S_L$ conditional on $\tilde{c}$ across the flame brush, for predictions of Eq. (16) with u'_Δ obtained from DNS and optimum values of β_c (i.e. $\beta_c = 3.3$ and 4.35 is used for cases A and B-F respectively); u'_Δ evaluated using Eq. (10) and optimum values of β_c (i.e. $\beta_c = 2.86$ and 3.7 is used for cases A and B-F respectively) and u'_Δ evaluated using Eq. (10) and β_c is evaluated using Eq. (19) at $\Delta \approx 0.8\delta_{th}$ (1st column) and $\Delta \approx 2.8\delta_{th}$ (2nd column) for cases A-F.

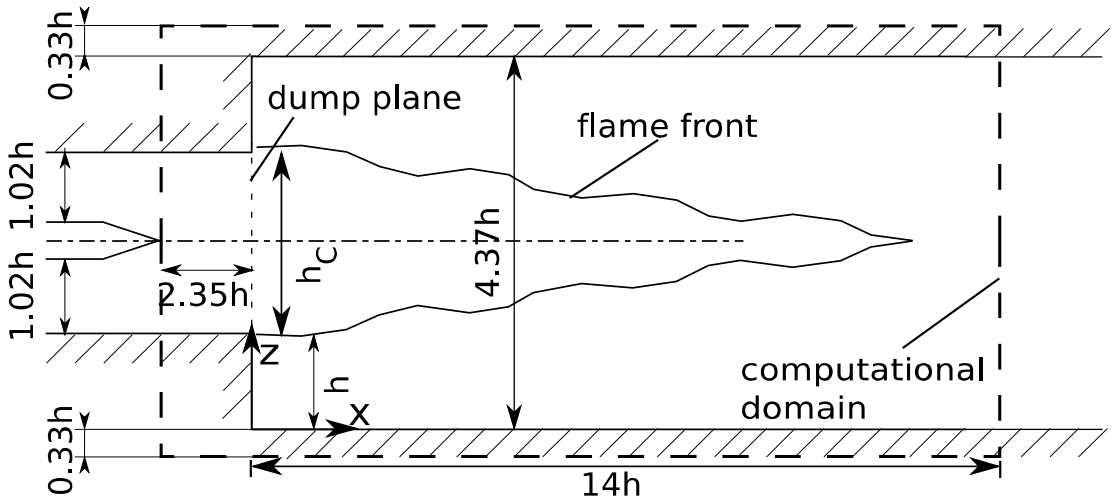

Figure 6: 2-D sketch of the ORACLES burner's combustion chamber, where *h* = 29.9mm. Interior width in the y-direction is 5.03*h*.

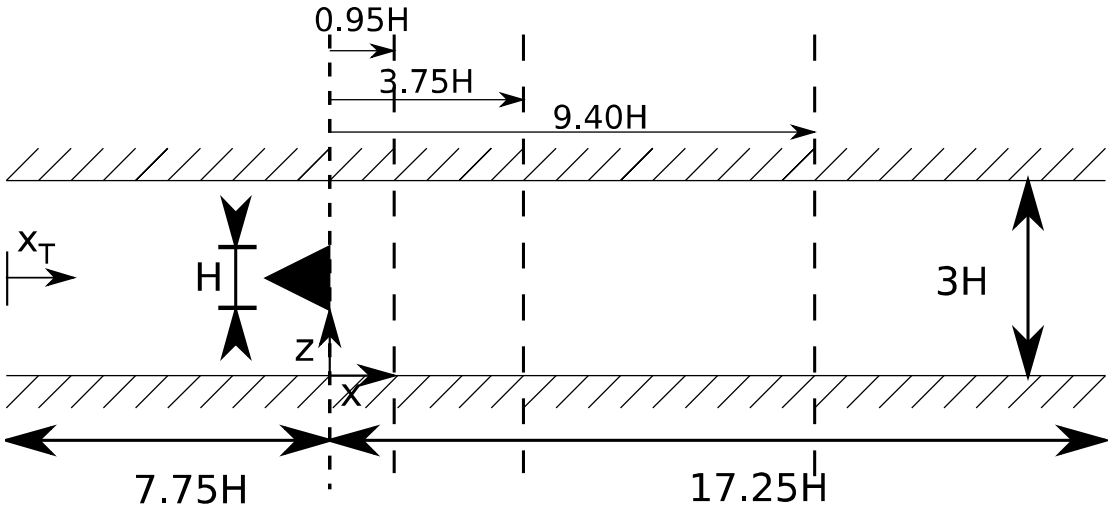

Figure 7: Sketch of the Volvo Rig's combustor, where *H* = 40mm. Interior width in the y-direction is 6*H*.

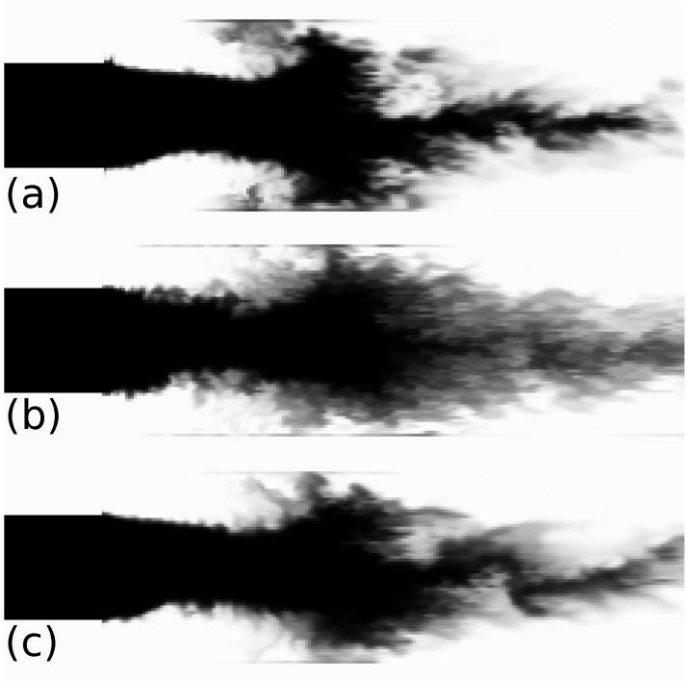

Figure 8: Instantaneous flame visualisations predicted by (a) SDR, (b) FurebyM and (c) Muppala models for the ORACLES burner.

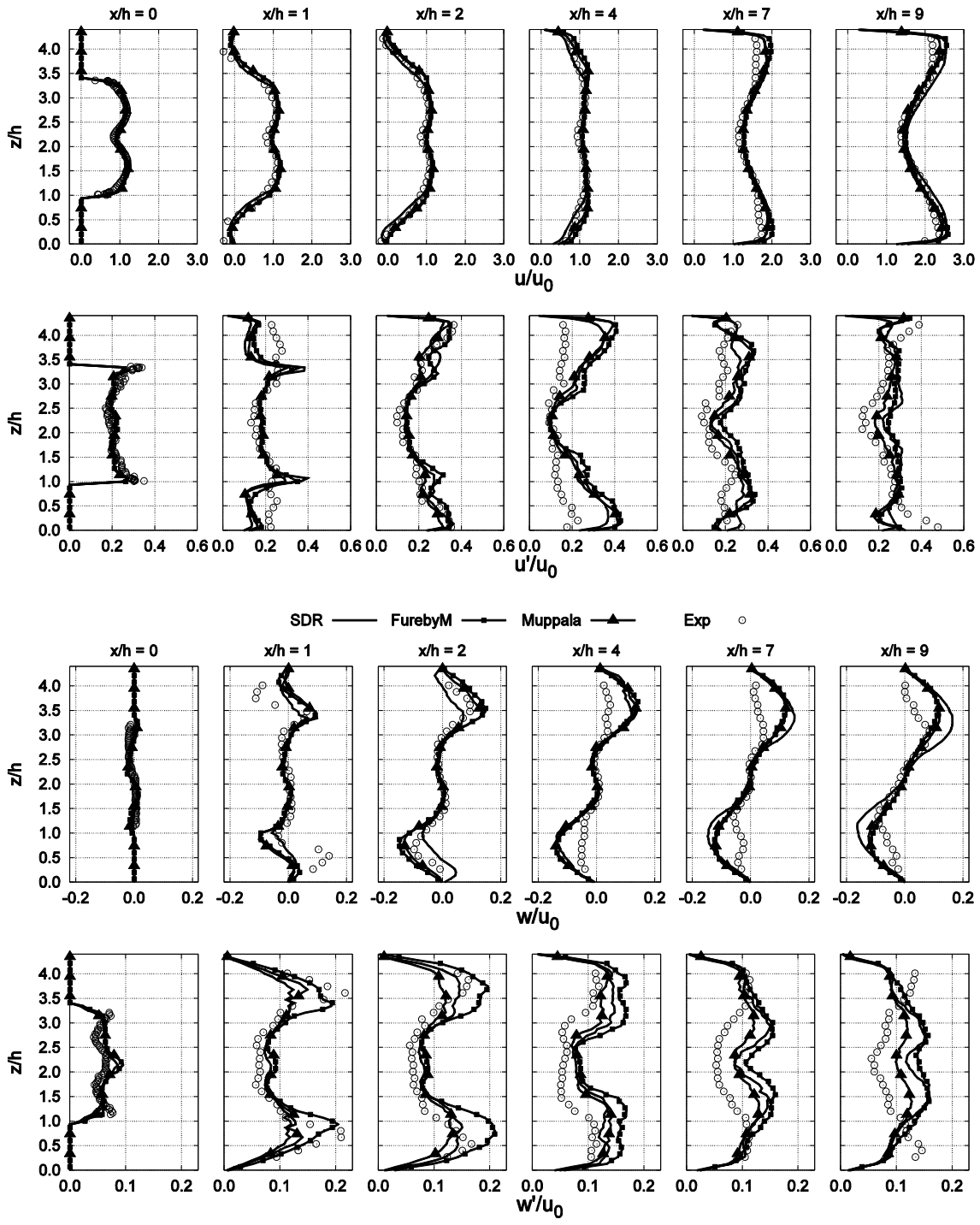

Figure 9: Normalised mean and fluctuating velocities predicted by SDR, FurebyM and Muppala models for the ORACLES burner.

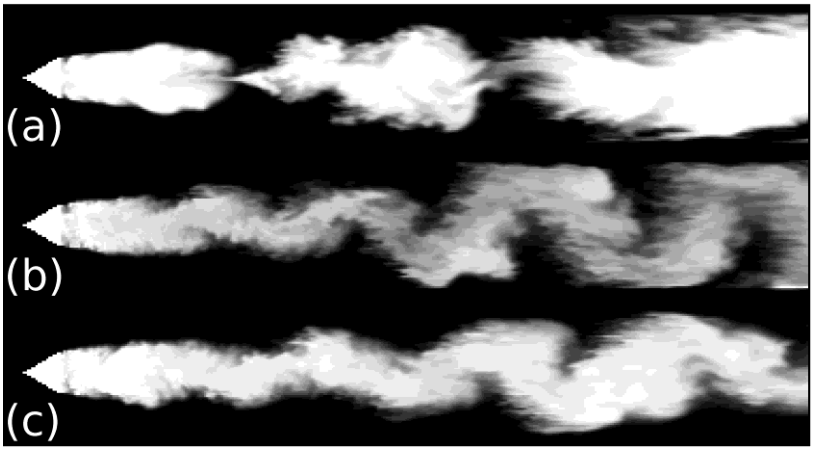

Figure 10: Instantaneous flame visualisations predicted by (a) SDR, (b) FurebyM and (c) Muppala models for the Volvo Rig.

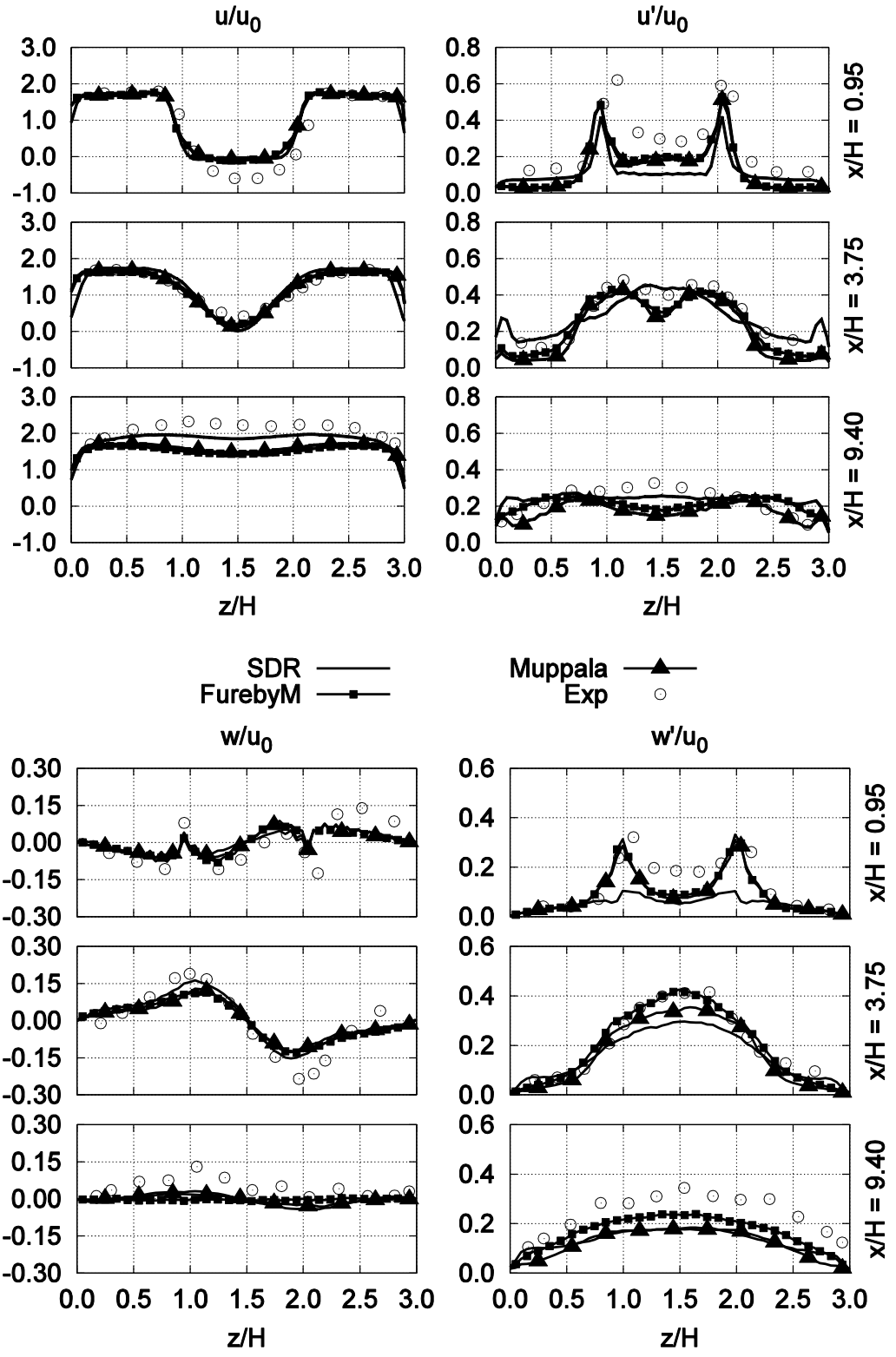

Figure 11: Normalised mean and fluctuating velocities predicted by SDR, FurebyM and Muppala models for the Volvo Rig.

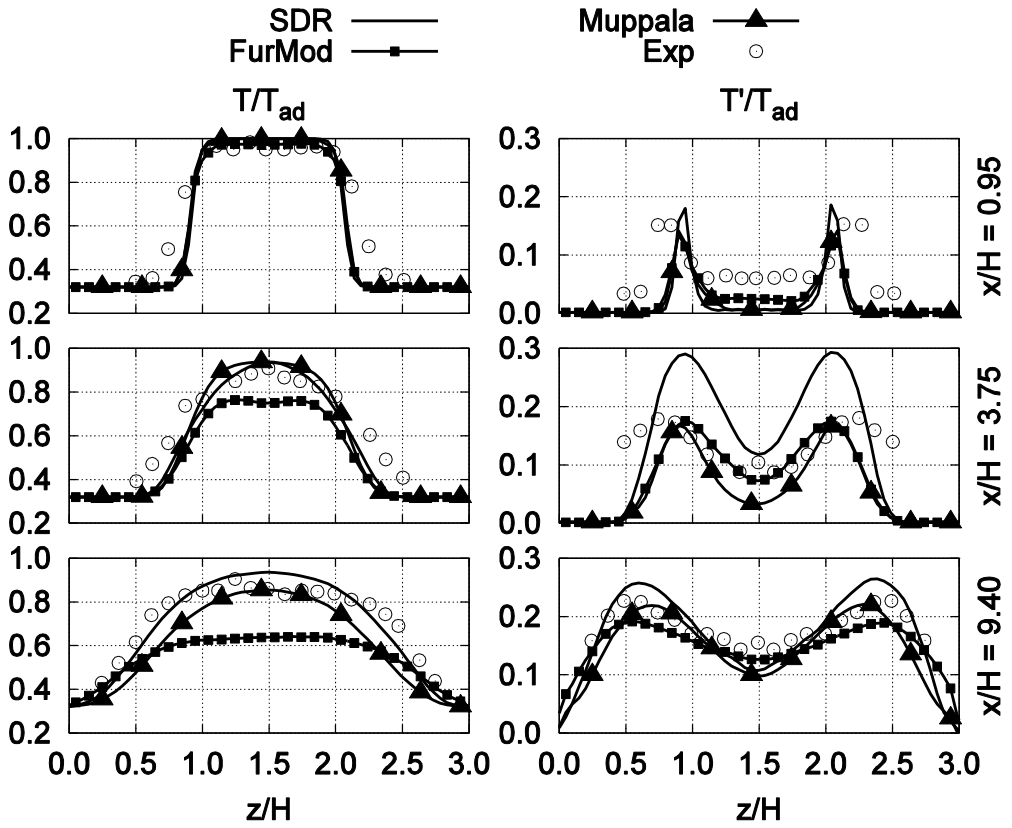

Figure 12: Normalised mean and fluctuating temperatures predicted by SDR, FurebyM and Muppala models for the Volvo Rig.

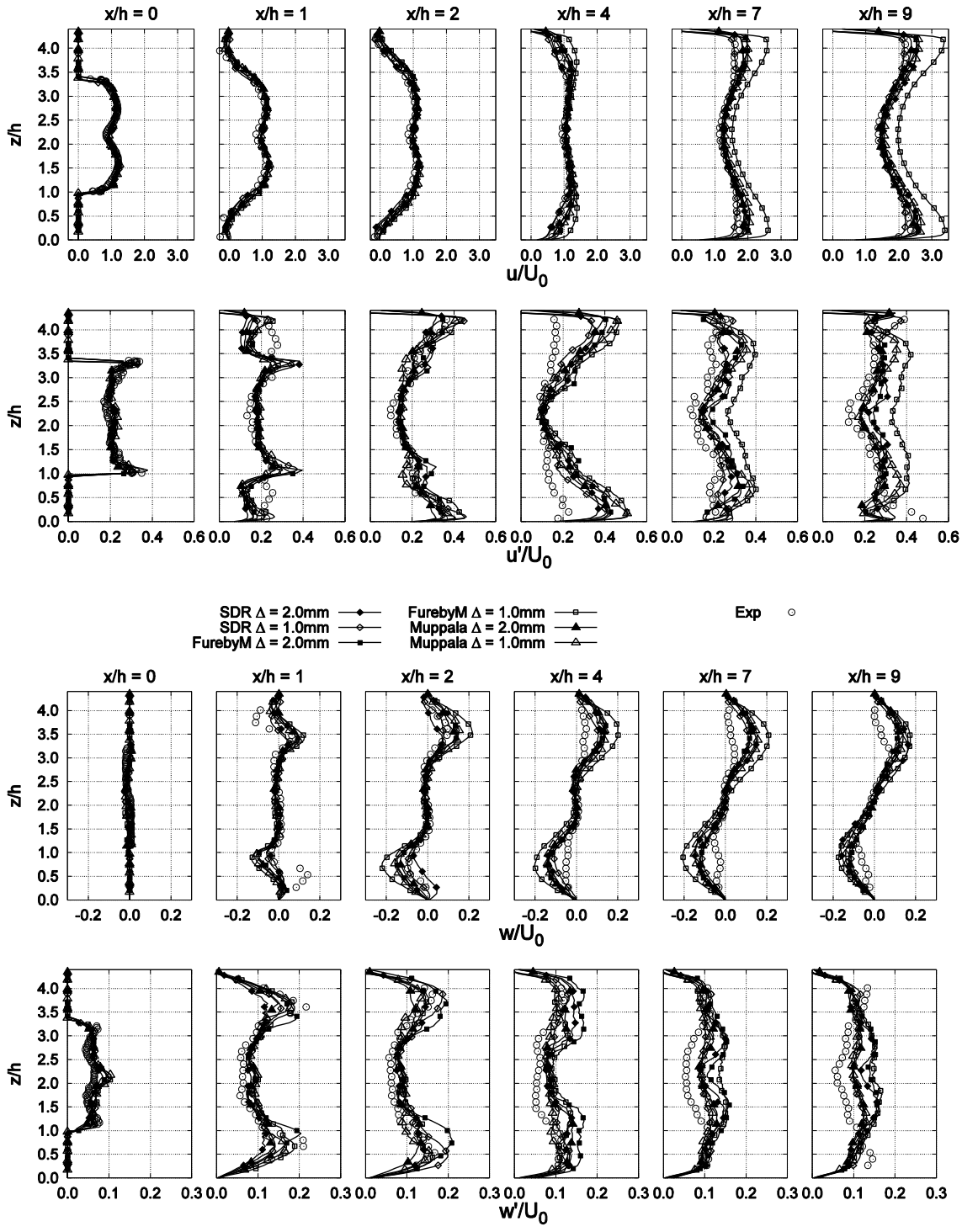

Figure 13: Normalised mean and fluctuating velocities predicted by the SDR based closure and FSD models using coarse and fine grids for the ORACLES burner.

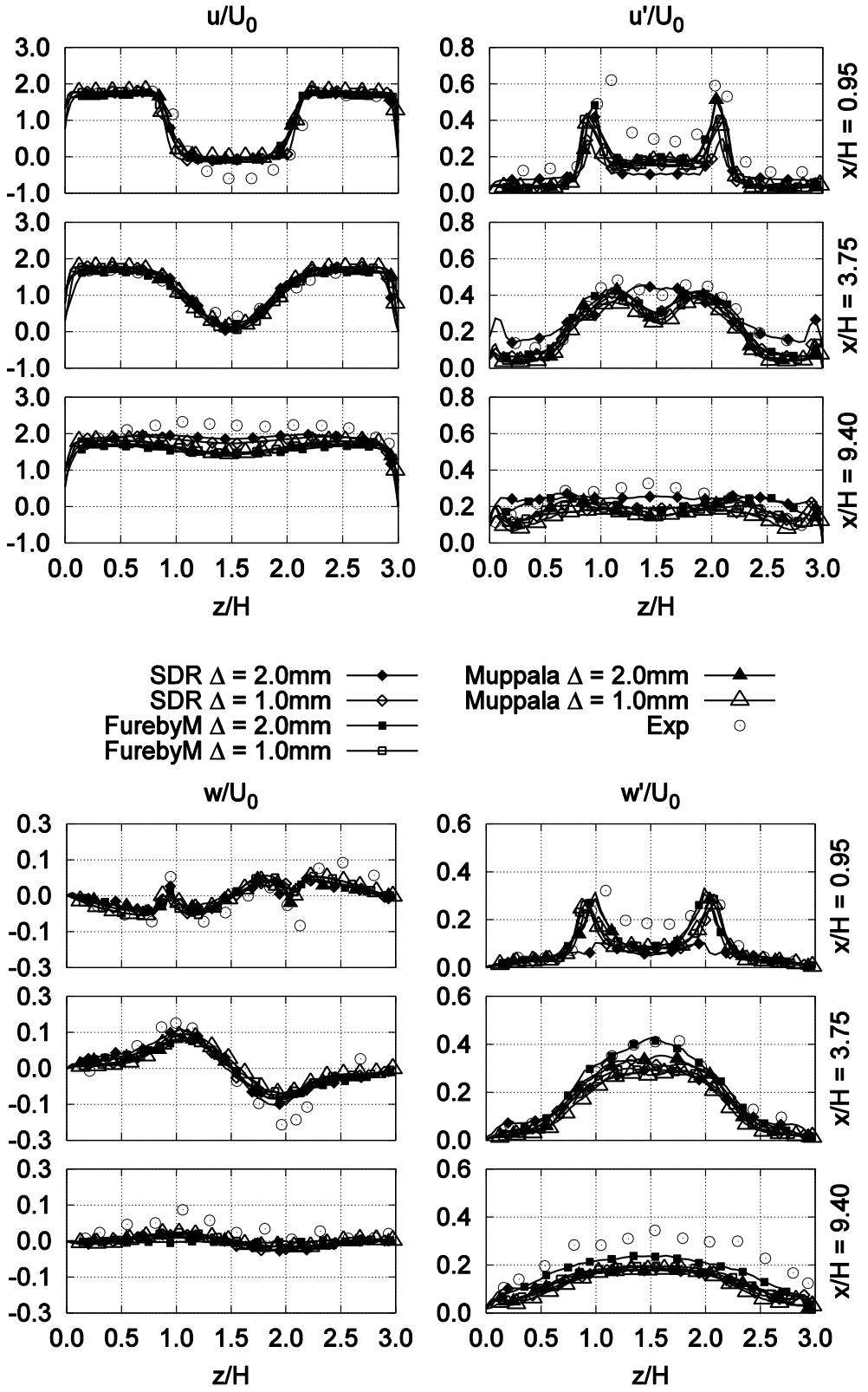

Figure 14: Normalised mean and fluctuating velocities predicted by the SDR based closure and FSD model using coarse and fine grids for the Volvo Rig.

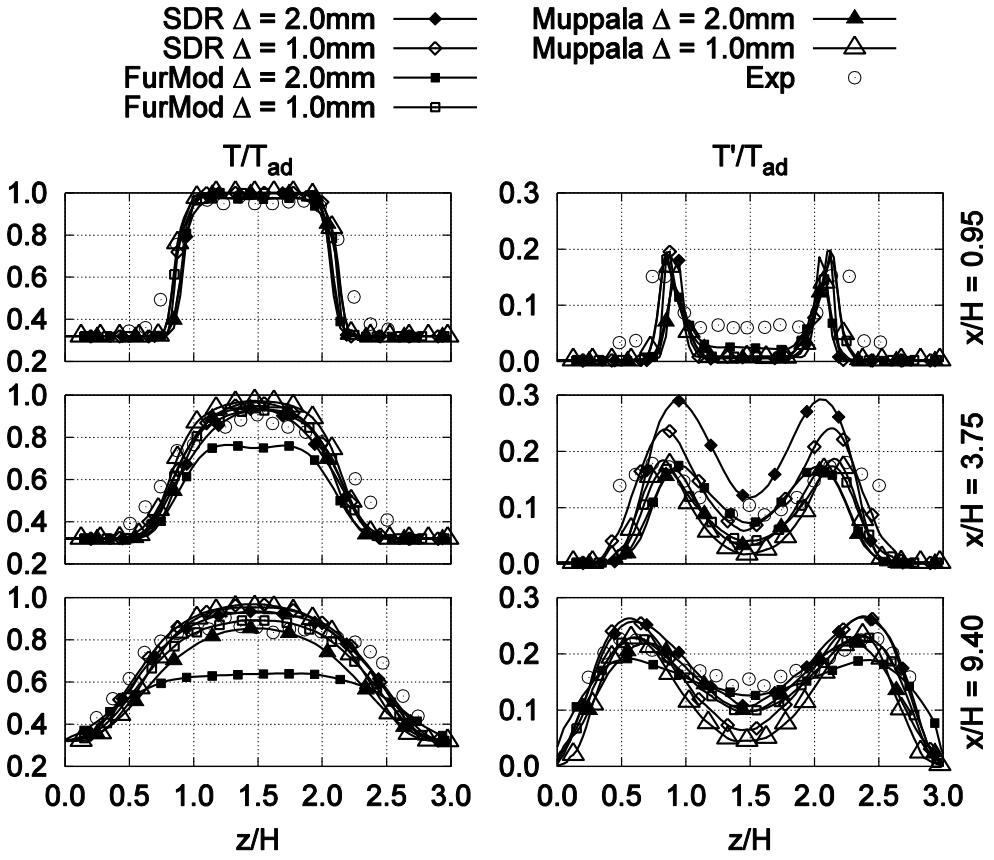

Figure 15: Normalised mean and fluctuating temperatures predicted by the SDR based closure and FSD models using coarse and fine grids for the Volvo Rig.

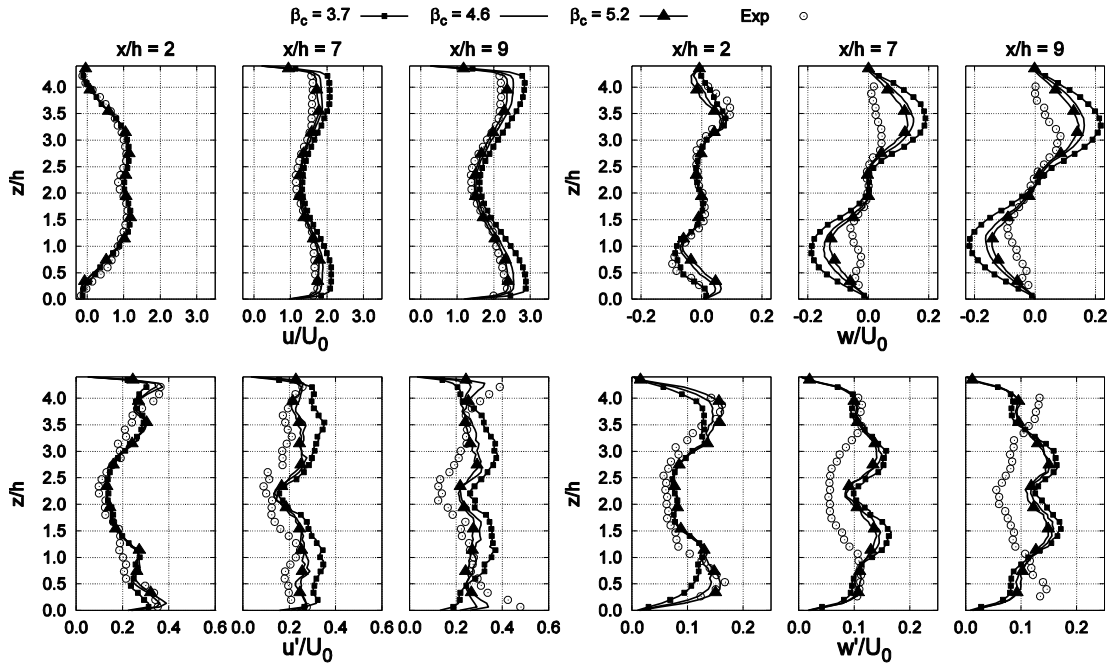

Figure 16: Normalised mean and fluctuating velocities predicted by $\beta_c = 3.7$, $\beta_c = 4.6$ and $\beta_c = 5.2$ at locations $x = 2h$, $x = 7h$ and $x = 9h$ for the ORACLES burner.

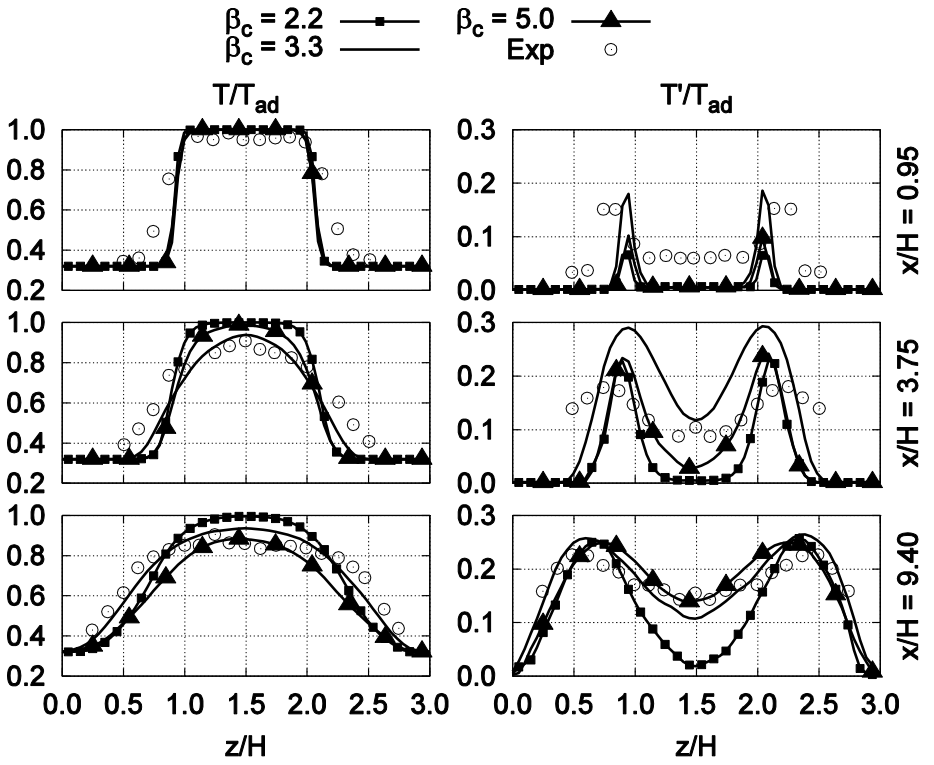

Figure 17: Normalised mean and fluctuating temperatures predicted by $\beta_c = 2.2$, $\beta_c = 3.3$ and $\beta_c = 5.0$ for the Volvo Rig.

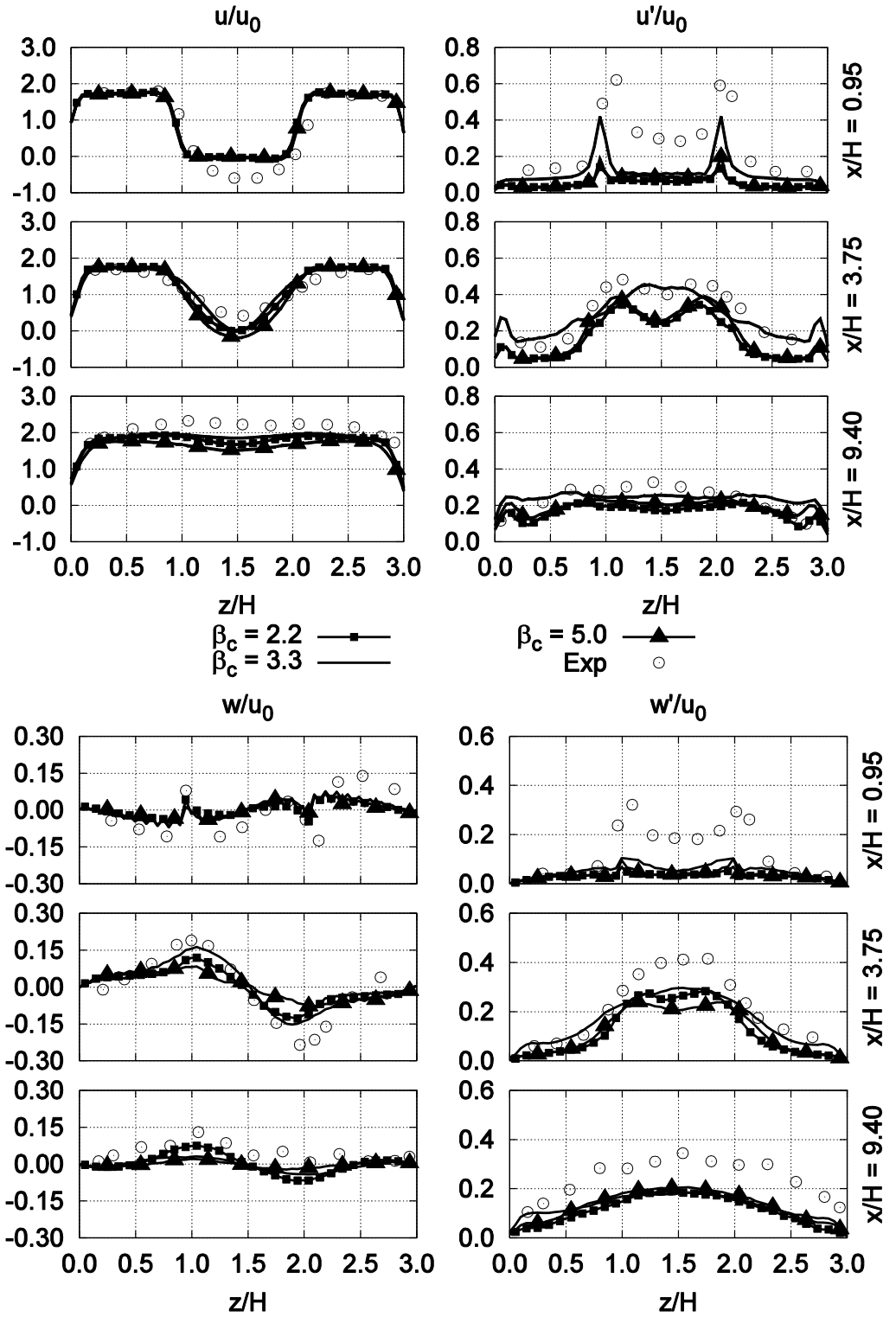

Figure 18: Normalised mean and fluctuating velocities predicted by $\beta_c = 2.2$, $\beta_c = 3.3$ and $\beta_c = 5.0$ for the Volvo Rig.